MAGNETIC TAPE RECORDING

HISTORY

In 1888, Oberlin Smith published an article, "Some possible forms of a phonograph." Oberlin Smith had already carried out the work in 1878, inspired by the telephone invented by Bell in 1877. In his paper, Smith described the basic principle of magnetic recording as it is used today. To record, he suggested leading small steel particles on a cotton thread through a coil. The coil carries a current proportional to a sound signal. For playback, the cotton thread is led through the coil again and an apparatus similar to Bell's telephone can reproduce the recorded sound. Oberlin Smith did not receive much recognition, though, because he had no functional device. A Danish engineer, Valdemar Poulsen, constructed the first recorder, the *Telegraphon,* in 1898. At the Paris World Exhibition in 1900, Valdemar Poulsen impressed the community with a recording of sound. Poulsen used a thin steel wire as recording medium.

Since there were no suitable electronics to amplify the signal, the Telegraphon did not gain importance for sound recording in the following years. After the invention of the vacuum tube, devices similar to the Telegraphon indeed recorded sound on steel tapes as Poulsen had suggested earlier. The steel tapes were heavy, clumsy to handle, and expensive. Fritz Pfleumer—who wanted to extend the use of his new cigarette paper manufacturing process—glued small iron particles onto his paper and created the first magnetic tape. (Fritz Pfleumer was actually not the first to have this idea: the American Joseph O'Neill had already applied for a patent in 1926, one year before Fritz Pfleumer.) The paper, however, tore readily, and Pfleumer decided to get help from the industry to commercialize his idea. An alliance between Allgemeine Elektrizitätswerke Gesellschaft (AEG) and Badische Anilin und Soda Fabrik (BASF) formed, in which AEG developed the recording device, and BASF developed the tape. In 1935, they presented the Magnetophon, which made use of a "ring head" that Eduard Schueller had invented during the development. BASF had replaced the paper substrate by a plastic base film. These two components improved the mechanics of the recorder significantly. Finally, the independent discovery of ac bias in Germany, Japan, and the United States in the late 1930s led to a large improvement of the sound quality of the recordings. The magnetic tape also improved. The carbonyl iron particles used for the Magnetophon tape were replaced by magnetite (Fe_3O_4) and later by γ-Fe_2O_3. Today needle-shaped γ-Fe_2O_3. particles are still used, but improved materials are needed for high-density recording. Apart from audio recording, magnetic tape has also found wide application in analog video recording, as well as digital data recording.

MANUFACTURING AND STRUCTURE OF TAPES AND FLOPPY DISKS

Particulate Tape: Structure and Manufacturing Process

Figure 1 shows a schematic cross-section for a *particulate tape.* A particulate tape consists of a base film, a back coating, and the magnetic layer. The base film is typically made of polyethyleneterephtalate (PET), with a thickness down to 7 μm. If a thinner base film is required, materials with a higher Young's modulus, such as polyethylene-2,6-naphthalate (PEN), have to be used. High-density recording is only possible if the magnetic surface is very smooth, which, in turn, presupposes a smooth base film. A tape wound with a lubricating film of air drawn in between the smooth front and back surfaces is impossible to handle, so the back coating is designed to provide a controlled surface relief. It should have an undulating rather than jagged structure so as not to damage the recording surface with which it comes into contact. In addition, the back coating is filled with conducting carbon black powder to counter the build-up of electrostatic charges. The relatively rough base film used for audio cassettes does not require a back coating. In addition to a magnetic powder, the typical recording layer contains carbon black, abrasive particles of Al_2O_3, dispersants, and lubricants, all held in a plastic binder consisting of a thermoplast and a polyurethane, together with an isocyanate cross-linking agent. The magnetic powder accounts for 20% to 50% in volume of the recording layer. The reader can obtain more information from Refs. 1–5.

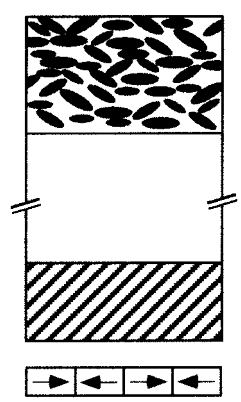

Figure 1. Cross-sectional view of the structure of a particulate tape. The magnetic layer typically contains needle-shaped particles together with a binder system. Particulate media are longitudinally magnetized.

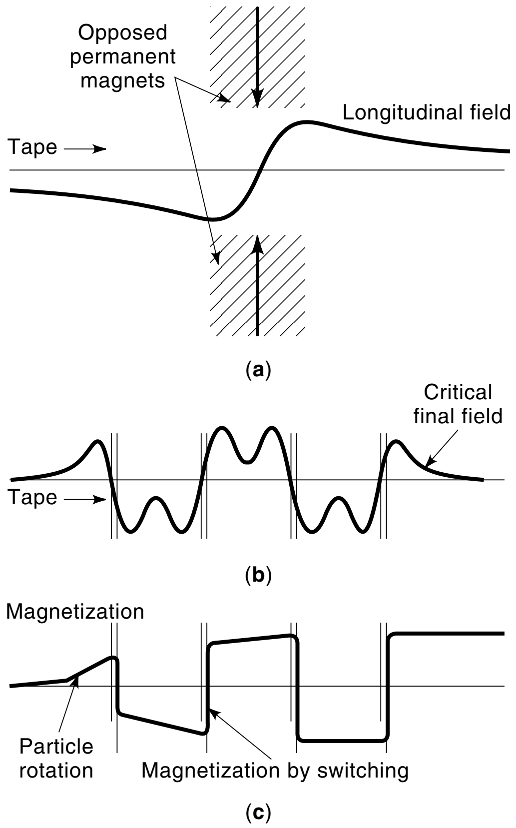

Figure 2. (a) A single orienting magnet consists of a pair of opposing permanent magnets, which are vertically oriented. An orientation with a multistage magnet is best if the field polarity changes sufficiently rapid for the magnetic moments to switch before the particles have time to rotate, (b) and (c).

The first stage in preparing the coating is to disperse the particles and so forth in a solution of the binder polymers. Vertical or horizontal bead mills, employed singly or in cascade, are standard dispersing equipment. Very fine particles, such as metal powder, can be better dispersed if a high-shear premix or kneading stage is added to the process. Just before coating, the cross-linking agent is added to the ink. Gravure, extrusion, or knife coating heads are used to put the ink onto the base film at web speeds between 100 m/min and 1000 m/min. Shortly after leaving the coating head, the still wet coating is magnetically oriented along the tape direction. Floppy disks are an exception: because they must be isotropic, it may be necessary to disorient them to remove any unwanted alignment due to shear in the coating head.

The most straightforward orienting magnet consists of two opposed permanent magnets [Fig. 2(a)], arranged symmetrically about the tape web, so that the wet coating sees only a longitudinal field. For better orientation, a sequence of such magnets may be installed. Figure 2(b) shows the resulting spatially alternating field. Orientation occurs if the polarity changes are sufficiently rapid for the magnetic moments of the particles to be switched around before the particles themselves have time to rotate, [see Fig. 2(c)]. This condition can be easily met for standard iron oxide and chromium dioxide tapes, but not for high-coercivity and high-moment metal particles (MP), which can be better oriented in the more unidirectional fields of large solenoids.

After the alignment, the coating has to dry until the chemical reactions in the binder system are (mostly) complete. The next step is to "calander" the tape. A calander presses the tape between polished rollers at a high temperature. This treatment results in a compressed magnetic film and, most important, in a very smooth surface finish. Finally, the tape is slit into the desired width and wound onto reels into cassettes. In the case of floppy disks, the "cookies" are punched out after calandering and mounted into their plastic housing.

Recording Particles

Only five magnetic materials are in use for particulate media:

1. *Maghemite* (γ-Fe_2O_3) is the light-brown material found on open-reel computer tapes, studio audiotape, and IEC I (International Electrotechnical Commission) audiocassettes. It is the lowest coercivity (24 kA/m to 30 kA/m) and oldest of the magnetic tape particles, suitable only for low-density storage. No new systems are designed to use γ-Fe_2O_3.
2. *Chromium dioxide* (CrO_2) was the first higher coercivity powder to improve on γ-Fe_2O_3 and established the "Chrome position" for audio cassettes. Most CrO_2 is now used in VHS (video home system) videotape, with smaller amounts going into IEC II audio and computer cartridge tape. Coercivities lie in between 40 kA/m and 60 kA/m, whereby CrO_2 tapes may have lower coercivities than equivalent Co modified γ-Fe_2O_3 tapes (see also the section titled Thermally Activated Magnetization Reversal Processes).
3. *Cobalt modified iron oxides* use the anisotropy of the cobalt ion to achieve coercivities of 30 kA/m to 80 kA/m. They are used in large quantities for consumer videotape, IEC II audio cassettes, QIC data cartridges (quarter inch cartridges), and floppy disks.
4. Doped *barium ferrite* (BaFe) has sometimes been hailed as the future high-density recording medium but, despite much development of experimental products, has so far appeared only in very small amounts in floppy disks.
5. *Metal particles* (MP) found their first significant application in high-output IEC IV audiotapes, but the main use is now in broadcast videotape as well as 8 mm consumer video, DAT (digital audio tape), data tape, and floppy disks. Since their introduction for video and DAT, the improvement in MP has been so spectacular that MP now dominates in new digital tape applications. The coercivity of video and digital MP ranges between 110 kA/m to 200 kA/m.

Table 1 summarizes magnetic properties of the powders used in tape and some other materials of interest.

Ferric Oxide (γ-Fe_2O_3). The essential problem in preparing ferric oxide, γ-Fe_2O_3, as well as Co-modified γ-Fe_2O_3 and metal particles, is to make uniaxially anisotropic particles from materials with cubic anisotropies and crystal habits. [As will be explained in the section "Magnetization Reversal in Fine Particles," elongated particles show the desired magnetic properties for tape.] Direct precipitation gives isometric particles, so a roundabout route, as illustrated in Fig. 3, via trigonal

Table 1. Material Properties for Some Magnetic Materials and Powders Used in Tape Manufacturing

	Magnetic Materials			Powders Used in Tape			
Material	σ_s (Am^2/kg)	M_s (kA/m)	ρ (g/cm^3)	σ_s (Am^2/kg)	H_c (kA/m)	Length (nm)	Diameter (nm)
γ-Fe_2O_3	76	350	4.6	73–75	24–30	250–500	30–50
Fe_3O_4	92	480	5.2				
CrO_2	106	490	4.6	75–85	35–60	250–320	30–45
$CoFe_2O_4$	80	425	5.3				
Co-doped γ-Fe_2O_3, (CoFe)				70–78	30–80	180–400	25–45
$BaFe_{12}O_{19}$[a]	72	380	5.3				
Doped $BaFe_{12}O_{19}$, (BaFe)[a]				55–65	50–120	10–40	40–100
Fe[b]	218	1710	7.8	120–150	90–200	60–250	20–40

[a] Platelet shaped.
[b] Tape particles here are oxide shell and may contain Co.

α-Fe_2O_3, must be followed to produce the desired acicular form. Three methods are in use to synthesize the α-Fe_2O_3, the most common being the dehydration of needles of FeOOH. Goethite, α-FeOOH, is formed by precipitation from a solution of $FeSO_4$ with NaOH. The second method is via lepidocrocite, γ-FeOOH precipitated from a solution of $FeCl_2$. In both cases, the next stage is the same, the dehydration to α-Fe_2O_3 at temperatures up to 800°C. To maintain the needle shape of the particles during dehydration, the FeOOH must be coated with some anti-sintering agent such as a phosphate. The third method is the direct hydrothermal synthesis of α-Fe_2O_3 from a suspension of $Fe(OH)_3$ using crystal modifiers to control the particle morphology. By avoiding the large density change on dehydration, the direct process introduces fewer of the defects and grain boundaries normally found in γ-Fe_2O_3 particles. Inhomogeneities give rise to internal magnetic poles which degrade the particle properties, and their absence has lent the direct-process particles the name *nonpolar* (NP). In hydrogen, or using a combination of hydrogen and organic compounds that can further hinder sintering, the α-Fe_2O_3 is reduced to magnetite, Fe_3O_4, at temperatures below 500°C. Magnetite has a higher magnetization than γ-Fe_2O_3 and is, at first sight, an attractive recording material. It has, however, proved unsatisfactory, because in a finely divided form, it oxidizes naturally to γ-Fe_2O_3. It is also more susceptible to print-through (see the section titled Thermally Activated Magnetization Reversal Processes). γ-Fe_2O_3 is a metastable form, which reverts to hematite (α-Fe_2O_3) on heating to 400°C, so the final oxidation of Fe_3O_4 to γ-Fe_2O_3 must not exceed approximately 350°C. A densification process to improve the handling properties is commonly applied to the finished particles.

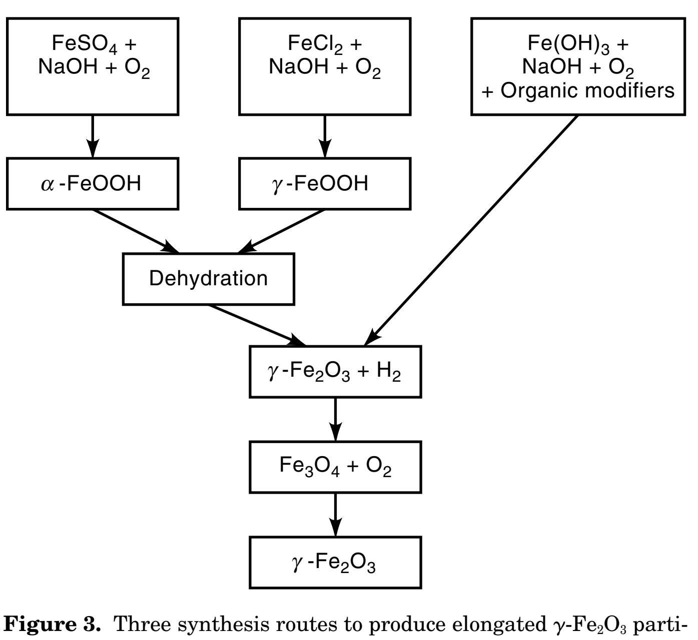

Figure 3. Three synthesis routes to produce elongated γ-Fe_2O_3 particles. The roundabout routes are necessary to grow elongated particles from materials with cubic crystal habits.

Typical particle lengths are 0.3 μm for the goethite and NP, and 0.4 μm for the lepidocrocite processes. The lepidocrocite particles tend to form bundles, which can be more easily oriented and packed, while the NP particles are very uniform and suitable for high-quality audio applications. About three-quarters of γ-Fe_2O_3 is prepared by the goethite process, which is also the basis for the manufacture of cobalt-modified oxides and metal particles.

Chromium Dioxide (CrO_2). In contrast to the iron oxides, CrO_2 is crystallized in a single-stage hydrothermal process. It has the rutile structure and forms smooth-faced acicular single-crystal particles. They tend to occur in parallel bundles and can be very well oriented. In addition to its shape anisotropy, CrO_2 has magnetocrystalline anisotropy. Chromium dioxide is an unusual material, being a ferromagnetic oxide and a good electrical conductor.

Synthesis of CrO_2 involves a reaction of an aqueous paste of CrO_3 and Cr_2O_3 under hydrothermal conditions. First, a thick mash is prepared and then heated in an autoclave to 300°C at a pressure of 350 MPa. The reacted product is a solid black mass, which must be drilled out of the reactor cans. It is then dispersed and treated with Na_2SO_3 or NaOH solution to topotactically convert the outer layer of the particles to β-CrOOH. This treatment is necessary to improve the stability of the powder in the presence of water but, as in the case of MP, it reduces the magnetization. The shape, size, and coercivity of the particles can be controlled by additives. Antimony and tellurium are used to vary the particle size, and iron to control the coercivity, although the iron doping also has an effect on the particle geometry. Up to about 3% of Fe^{3+} can be incorporated into the CrO_2 structure, increasing the magnetocrystalline anisotropy and the coercivity to over 80 kA/m. Between the Fe and Cr the exchange coupling is antiferromagnetic and stronger than the Cr–Cr exchange. Consequently, Fe doping decreases the saturation magnetization of CrO_2, while increasing the Curie point from 118°C for undoped material to about 170°C. Iridium is the most effective dopant for CrO_2, producing a spectacular rise of coercivity up to 220 kA/m. Although this material remains an expensive laboratory curiosity, mixed doping with very low levels of Ir can be used commercially for high-coercivity powders.

Cobalt-Modified Iron Oxides (CoFe). Cobalt-modified iron oxides (CoFe) utilize the high anisotropy of the Co^{2+} ion to increase the coercivity of the iron oxides described above. There are two classes of CoFe powders.

1. *Bulk Doped.* The most straightforward way to add cobalt is to deposit Co hydroxide onto either the γ-FeOOH or α-Fe_2O_3, and then to proceed with the normal heat treatments. The Co diffuses into the body of the particle. For lower quality applications of powders up to about 50 kA/m, this procedure is adequate, but it has certain weaknesses. The anisotropy and coercivity are strongly dependent on temperature, are subject to magnetostrictive losses, and demonstrate strong magnetic annealing effects. The latter is due to the well-known tendency of Co^{2+} ions to form pairs or groups ordered along the direction of magnetization. Therefore, the coercivity drifts with time, and because the particles adjust to local magnetic fields of the recorded signal, erasure is poor.
2. *Surface Modified.* Rather than treating the precursors, a 1 nm to 2 nm coating of $CoFe_2O_4$ is formed on the γ-Fe_2O_3 particle. No high temperatures are encountered and the Co remains at the surface. There are two methods of preparation. In the adsorption technique, cobalt hydroxide is precipitated onto γ-Fe_2O_3 and a portion of the cobalt is incorporated into the surface layer of the oxide. In the epitaxial method, cobalt ferrite from a mixture of Fe and Co solutions is precipitated directly onto γ-Fe_2O_3. Despite the anisotropy of $CoFe_2O_4$ being cubic, the dominant effect of the coating is to increase the uniaxial anisotropy of the particle. This is not properly understood, but could, for example, be due to stress or ordering effects at the boundary. The instabilities of bulk-doped material are roughly halved in importance by the surface modification, and such powders coat the majority of IEC II audio tapes, VHS, and S-VHS videotapes as well as floppy disks and QIC data cartridges.

Barium Ferrite (BaFe). Barium ferrite ($BaFe_{12}O_{19}$) has the M-type hexaferrite structure and a large uniaxial magnetocrystalline anisotropy (H_A = 1350 kA/m) directed along the hexagonal axis. Barium ferrite forms flat plates perpendicular to the easy axis in which the shape anisotropy, in contrast to other recording materials, works to reduce the coercivity. The pure form, with coercivities in the range of 300 kA/m, is used in credit card stripes and the like, but for tape applications, only doped material with lower coercivity has been used. Substituting elements such as Co^{2+} and Ti^{4+} for some of the Fe^{3+} adjusts the coercivity to the range of 50 kA/m to 200 kA/m and reduces the otherwise problematic temperature variation of the coercivity.

The ceramic method of firing and milling used to make barium permanent magnets is unsuitable for fine recording particles for which two methods are in use. In the *hydrothermal process,* the metal hydroxides are precipitated from salt solutions with an excess NaOH, and the resulting suspensions are heated in an autoclave to 200°C to 300°C. The washed-and-dried product is then annealed at 700°C to 800°C, to increase the magnetization. In the *glass crystallization process,* the components for the desired barium ferrite are dissolved in a borate glass melt. After rapid quenching, the amorphous glass flakes are annealed at temperatures up to 800°C. Last, the glass matrix is dissolved to separate the barium ferrite particles. Both methods can produce platelets of 50 nm and smaller in diameter. It can be observed that the magnetization decreases for very thin platelets, which is attributed to a 'dead layer' at the surface. One way to increase the magnetization is to deposit magnetite on the surface.

From its shape, barium ferrite appears to be the ideal powder to make vertically oriented media, especially floppy disks. However, the difficulty in producing a vertically oriented coating with a smooth surface, the tendency for the flat particles to stack together, and problems with the mechanical integrity of the coatings, have hindered its widespread introduction. The new, much smaller MP particles have also eroded barium ferrite's one-time advantage in theoretical signal-to-noise ratio. The main advantage remaining to barium ferrite is its stability against corrosion.

Metal Particles (MP). Metal particles (MP) are prepared from γ-Fe_2O_3 precipitated from $FeSO_4$. Three generic processes may be defined, although the actual manufacturing process may involve some combination of these: *basic process,* a solution of $FeSO_4$ is added to an excess of NaOH in solution, $pH > 7$; *acid process,* the $FeSO_4$ and NaOH are mixed in stoichiometric proportions, $pH < 13$ (in the range $7 < pH < 13$ cubic magnetite is precipitated instead of γ-FeOOH); *carbonate process:* $FeSO_4$ is added to an excess of Na_2CO_3. The basic and acid processes both produce cylinder-shaped γ-FeOOH, while the carbonate process leads to so-called "spindle-shaped" particles. The spindle-shaped particles are actually fine fibers of FeOOH forming bundles with tapering ends and can be much smaller than the cylinders. Following precipitation and surface treatment, the next stages are similar to those for γ-Fe_2O_3, except that the reduction of the α-Fe_2O_3 in H_2 is carried through to the metal. The pure metal powder is pyrophoric and cannot be used, so a controlled oxidation of the surface is carried out at 80°C to 100°C to generate a passivation layer, approximately 4 nm thick. Fe_3O_4 or γ-Fe_2O_3 can be identified by X-ray and Mößbauer analysis of the passivation layer. The crystallites are superparamagnetic at room temperature and do not contribute to the magnetic properties of the particles. It appears that a polycrystalline/amorphous layer can better accommodate the lattice mismatch between metal and oxide and forms a less permeable protective layer. Doping with nickel up to 3% and cobalt up to 30% increase the magnetization of iron and/or facilitate the reduction process. A Co content of 30% is standard in advanced metal particles.

MP is increasingly used in high-density recording systems, in which a very smooth tape surface is essential. It is crucial, therefore, to apply surface treatments at different stages of manufacture to prevent sintering, not only to preserve the particle shape and coercivity, but also to improve the dispersing properties. To this end, a combination of SiO_2, AlOOH, or rare-earth oxides may be deposited on the γ-FeOOH or α-Fe_2O_3. For further reading, see Ref. 5.

Particulate Tape: Double-Layer Coating

Although there have been early attempts, this technology did not receive much interest until very recently. Recent double-layer media have a very thin magnetic layer (MP), and a non-magnetic underlayer that contains very small TiO_2 or α-Fe_2O_3 particles (6). The two layers are coated simultaneously, whereby their rheological properties need to be adjusted properly. The first commercial product was a Hi 8 videotape with considerably improved recording performance. The thinness of the magnetic layer itself—which is about 400 nm for this tape—is not responsible for the increased output. The manufacturing process requires a certain minimum coating thickness, regardless of whether it is magnetic or not, to achieve smooth surfaces. Depending on the recipes used, either double or (thick) single layer coatings can be made smoother. Magnetically, thin magnetic layers have advantages in overwrite behavior

Meanwhile it has been demonstrated that magnetic layers as thin as 120 nm can be achieved (7,8). The most advanced MP double-layer tapes can compete with Metal Evaporated (ME) tapes. The application for these tapes is the digital video cassette (DVC), which is a tape system intended for digital video recording.

Thin-Film Tape: Structure and Manufacturing Process

Metal Evaporated (ME) Tape. Figure 4 shows a schematic cross-section of ME tape. ME tape consists of a base film, a back coating, the magnetic layer, a carbon protection layer, and a lubrication layer. While the back coating is virtually identical to those used for particulate media, the base film shows a distinct difference. The surface of the base film, onto which the magnetic layer is deposited, carries a thin coating

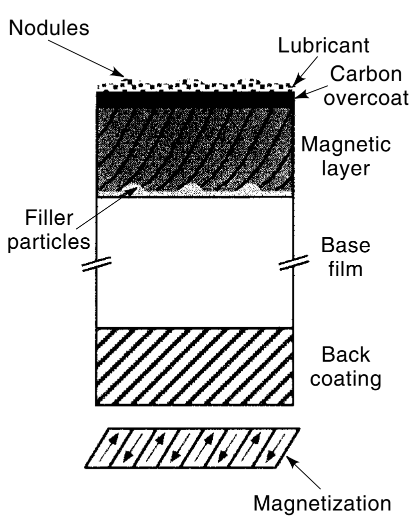

Figure 4. Cross-sectional view of the structure of a thin film tape (metal evaporated tape). A carbon overcoat and a lubrication layer protect the magnetic layer. The base film contains filler particles, which lead to nodules sticking out of the tape. The favored magnetization direction is oblique.

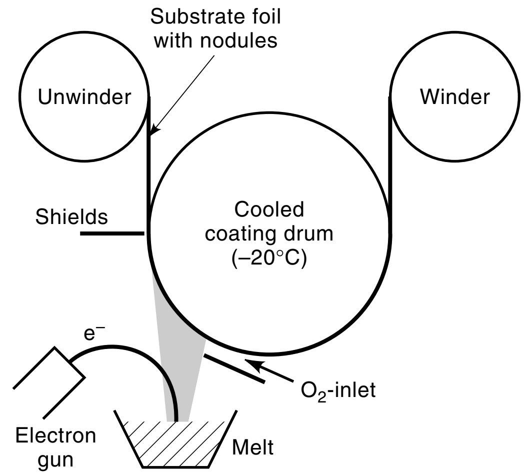

Figure 5. Sketch of a roll-coater used to manufacture ME tape. The magnetic alloy is heated with an electron gun and evaporated onto a base film that passes by. Oxygen is present during the evaporation process, which helps to isolate the magnetic grains.

with very small particles. After deposition of the magnetic film, the surface of the magnetic layer then shows 'nodules'. These nodules are about 10 nm to 20 nm high, and have a density of 10 to 50 per μm^2. The invention of the nodules has been the technological breakthrough for ME tape. The nodules improve tribology at the expense of an additional head to tape spacing loss, which sacrifices a bit of the recording performance.

Hi 8 ME tape is manufactured by oblique evaporation of a $Co_{0.8}Ni_{0.2}$ alloy in an oxygen atmosphere (9) (see Fig. 5). The typical composition of ME tape is about $(Co_{0.8}Ni_{0.2})_{0.8}O_{0.2}$ for the Hi 8 ME tape. Bulk $Co_{0.8}Ni_{0.2}$ has a 19% lower saturation magnetization than Co, and a comparable anisotropy field. Advanced ME tapes for DVC application contain no Ni (10). Due to its sufficiently high production speed (up to about 100 m/min) evaporation is—in contrast to sputtering—a suitable technology to produce videotapes. In the very beginning of the evaporation of the layer, the vapor arrives at the substrate at grazing incidence. A film grown at grazing incidence shows uniaxial anisotropy in an oblique direction (11,12). Roll-coaters operate in a wide range of evaporation angles [continuously varying incidence, (CVI) (9)]. The film deposition has to start at grazing incidence to preserve oblique anisotropy. A CVI process leads to a curved columnar microstructure, as sketched in Fig. 6. The magnetically easy axis is tilted out of the film plane. The tilt angle roughly coincides with the angle at which the columns start to grow on the base film. The columns themselves are not the relevant magnetic subunits for magnetization reversal and form a secondary structure (13). Individual crystals of ME tape are very small (about 5 nm in size). The magnetocrystalline anisotropy of the Co-alloy is the major source of anisotropy in ME tape.

Self-shadowing effects and low surface mobility (the substrate temperature is typically between −20°C and −30°C), lead to a formation of a very porous layer, especially at grazing incidence (14). The columns do not grow in the direction of the incoming beam. Due to the effect of shadowing, the growth direction is closer to the film normal. This can be ap-

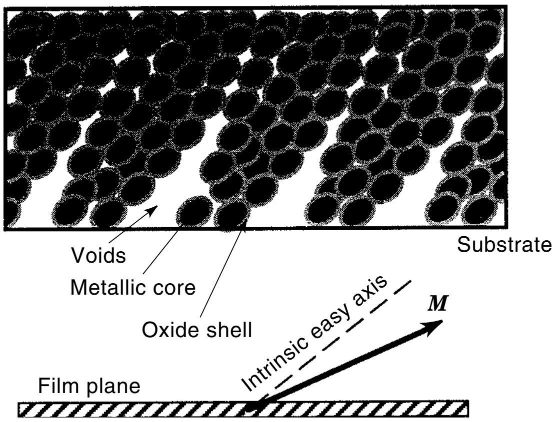

Figure 6. Sketch of the ME tape structure. Due to the oblique evaporation, the tape has a columnar structure. The magnetically easy axis is tilted out of the film plane. In zero field, the demagnetization energy pulls the magnetization closer to the film plane.

proximated by the "tangent rule":

$$\tan \alpha_c = 0.5 \tan \alpha_B \tag{1}$$

Here α_c and α_B are the angles that the column and the beam make with the film normal, respectively. At higher substrate temperatures, more continuous layers emerge, which are unsuitable for high-density recording. In case of ME tape, almost half of the volume of the magnetic layer consists of voids due to shadowing effects (13).

For improvement of particle separation and material yield, the evaporation is performed in the presence of oxygen. The oxidation of the magnetic material largely removes exchange coupling in ME tape, but there remains a magnetic correlation along the columns, which is also discussed in section titled Transition Models. Auger depth profiling shows the formation of oxide-rich surface and bottom layers. The upper oxide layer improves the mechanical performance of the tape, but lowers the output level due to the increased magnetic spacing between head and the active part of the medium. Another benefit of the upper oxide layer is corrosion protection of the tape. As indicated in Fig. 6, the "ME tape particles" are believed to have an oxide shell of CoO (and NiO) around a metallic core. Exchange anisotropy has been reported in ME tapes (15), which is consistent with this assumption.

The carbon protection layer is absent in some of the Hi 8 ME tapes. Advanced ME tapes utilize a Diamond Like Carbon (DLC) layer, to mechanically protect the tape. A layer thickness of 10 nm or even less is sufficient to improve wear resistance and provide additional corrosion protection for the metallic film (16). Since the protection layer is very thin, it can be sputtered in a separate station in the roll-coater. For improved runnability, the tape needs a lubricant layer. For particulate tape, it is believed that the lubricant forms a monomolecular layer on top of the coating. If worn off, the reservoirs inside the magnetic layer continuously replenish the lubricant. Since there are no pores on the surface of thin film media that can retain the lubricant, the lubricant must anchor itself to the thin-film surface.

Other Thin-Film Tapes. There have been many attempts to prepare thin-film media other than ME tape on flexible substrates. Co–Cr thin films having an easy axis of magnetization perpendicular to the film plane have been investigated intensively. From a production point of view, ME tape is better suited for videotape, because a vertical Co–Cr medium requires an additional magnetically soft underlayer. (For a discussion of vertical recording, see the section titled 'Magnetization and Demagnetizing Fields'.) Oblique evaporation of single-layered Co-Cr media for use together with a ring head has been suggested (17).

The vapor pressures of Co and Cr—unlike Co and Ni—are considerably different, which makes control of an evaporation process more difficult than in the case of ME tape. The basic challenge in preparation of Co–Cr media is to break up the exchange coupling between the individual magnetic subunits as far as possible. Perpendicular Co–Cr layers have a columnar structure with grain sizes of about one-tenth of the layer thickness, which typically ranges from 0.1 μm to 0.3 μm. The underlying mechanisms that cause the formation of more or less magnetically independent subunits are still under discussion. Up to now, good recording results were only reported for films prepared at high substrate temperature (200°C to 250°C). For flexible substrates (videotape), these high temperatures require the use of the expensive polyimide (PI) film as a substrate, rather than the cheaper PET film, which can be used for ME tape. Changes in composition inside the grain of Co–Cr films show characteristic patterns that have been named 'chrysanthemum-like' (18,19). Thin-film media on flexible substrates other than ME tape gained virtually no practical importance. Apart from the aspects discussed above, the poor tribological properties, especially for Co–Cr-based media, prevented any practical implementations. The reader can find more information on Co–Cr and vertical recording in Refs. 20–22.

MAGNETIC PROPERTIES OF TAPES

Magnetic Parameters

The various types of tape differ in magnetic properties. Figure 7 illustrates the most important magnetic parameters. The magnetic properties of tapes are typically measured with vi-

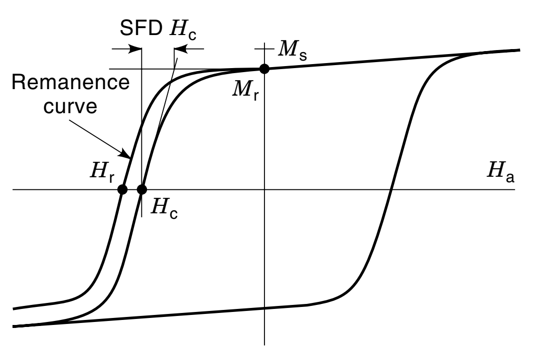

Figure 7. Hysteresis loop, remanence curve, and characteristic magnetic parameters. The saturation magnetization, M_s, is the maximum obtainable magnetization, the remanent magnetization, M_r, is the magnetization at zero field after saturation. The coercivity, H_c, is the field required to make the magnetization zero after saturation. The switching field distribution, SFD, defines how uniformly the medium switches. The remanent coercivity, H_r, gives the field, which makes the remanent magnetization zero after saturation.

brating sample magnetometers (VSM). These instruments measure the magnetization as a function of the applied field. The following properties characterize hysteresis loops:

- *Saturation Magnetization,* M_s. The saturation magnetization is the maximum attainable magnetization at very large applied field. The saturation magnetization for tape has to be distinguished from the saturation magnetization of the particles themselves. The tape magnetization is lower because the binder system (or voids) dilutes the magnetic material.
- *Remanent Magnetization,* M_r. The magnetization that remains after removal of a field. To avoid confusion, the remanent magnetization obtained after saturation with a large field is often referred to as *saturation remanence.*
- *Squareness.*

$$S_q = \frac{M_r}{M_s} \tag{2}$$

  In zero field, the magnetization of each particle will be on its easy axis. Since the particles in a tape are never aligned perfectly, and the measured magnetization is the magnetization component along on the field axis, it is smaller than the saturation magnetization, that is, $S_q \leq 1$. Therefore, the squareness reflects the degree of particle alignment. Magnetic interactions also tend to increase the squareness.
- *Orientation Ratio.* This is the ratio of the two saturation remanences in longitudinal (x) and transverse (y) direction. Since inhomogeneous magnetization within the particles at zero field can reduce the remanent magnetization, the orientation ratio captures the degree of particle alignment better than the squareness.
- *Coercivity.* The coercivity, H_c, gives the field at which the magnetization component along the applied field becomes zero.
- *Switching Field Distribution, SFD.* In magnetic tapes, there is a distribution of the switching fields of the particles. Köster has shown that the normalized slope of the hysteresis loop—which contains reversible and irreversible magnetization changes—is a convenient measure for the 'real' switching field distribution (23):

$$\text{SFD} = \frac{M_r}{H_c}\left(\frac{dM}{dH}\right)^{-1} \text{at } H = H_c \tag{3}$$

  The SFD is related to the normalized slope, S^*, by $\text{SFD} = 1 - S^*$.

The hysteresis loop contains reversible and irreversible magnetization changes. For information storage, only irreversible changes are of importance. *Remanence curves* can separate irreversible from irreversible magnetization changes. A point on the remanence curve is measured as follows: (1) magnetically saturate the sample, (2) apply a field in the opposite direction, (3) measure the magnetization with the field removed. The remanent magnetization plotted against the previously applied field value is the remanence curve (see Fig. 7). The field at which the remanent magnetization becomes zero is the *remanent coercivity,* H_r. In accordance with the theory, the remanent coercivity is somewhat larger than the coercivity. There are different definitions for the SFD, but it is common practice to use Eq. (3) for convenience.

Table 2 summarizes typical tape parameters for some applications. The well-established oxide media (γ-Fe_2O_3, Co-doped γ-Fe_2O_3, and CrO_2) show the smallest tape magnetization and coercivities. Tape data for the same pigment type can deviate considerably depending on the application. Although videotapes made of CrO_2 and Co-doped γ-Fe_2O_3 are compatible with one another, their coercivities do not agree. CrO_2 shows a stronger time dependence of the coercivity than Co-doped γ-Fe_2O_3, which leads to the same coercivity at recording (see also the section titled "Thermally Activated Magnetization Reversal Processes"). Table 2 illustrates that the more advanced tapes—such as MP and ME tape—have considerably more particles per unit volume. For further reading, see Refs. 1 and 3.

Magnetic Parameters of ME Tape

ME tape is prepared by oblique evaporation. Therefore, the magnetically easy axis of ME tape is tilted out of the film plane. It was realized early that the tilt of the easy axis makes the recording performance in one direction different from that of the other (see also the section titled "Transition Models"). Little attention was paid to the demagnetization effects present in simple measurements of the magnetic properties. Magnetic properties of regular particulate tapes are measured in longitudinal direction, which coincides with the alignment direction (i.e., the easy axis of the tape). This standard procedure yields low values for the squareness, S_q, and large values for the SFD for ME tape. Magnetically, ME tapes did not seem to be very attractive.

If the tape magnetization has a perpendicular component, there is a perpendicular demagnetization field that has to be added vectorially to the applied field. The magnetic 'particles' in the tape, therefore, do not 'see' the external field alone, but rather the vectorial sum of the external field, $\boldsymbol{H}_a$, and the demagnetizing field, $\boldsymbol{H}_d$:

$$\boldsymbol{H}_i = \boldsymbol{H}_a + \boldsymbol{H}_d \tag{4}$$

If the external field is applied at an angle ϑ_E, with ϑ_E being the angle between film plane and applied field, the internal field is:

$$H_{i\parallel} = H_i \cos\vartheta_i = H_a \cos\vartheta_E \tag{5}$$

$$H_{i\perp} = -H_i \sin\vartheta_i = -H_a \sin\vartheta_E - M_\perp \tag{6}$$

Eqs. (5) and (6) assume that the demagnetization factor perpendicular to the film plane is equal to one and the other demagnetization factors are zero. Therefore, the demagnetizing field is always perpendicular to the film plane and equal in magnitude to the perpendicular magnetization component, $M_\perp$.

Consider the case of a very large external field applied in film plane, which is subsequently removed. With no external field present, the sample is lying in its own demagnetizing field. During the removal of the external field, the internal field has not only changed its magnitude, but also its *direction,* namely, from an in-plane orientation to a perpendicular orientation. Evidently, sweeping the external field—as it is

Table 2. Magnetic Parameters of Various Tapes and Floppy Disks

Application	Type	M_r (kA/m)	H_c (kA/m)	Coating (μm)	n^b (1000/μm^3)
Reel-to-reel tape	γ-Fe_2O_3	100–120	23–28	10	0.3
Audiotape IEC I	γ-Fe_2O_3	120–140	27–32	5	0.6
Audiotape IEC II	CrO_2	120–140	38–42	5	1.4
	Co-γ-Fe_2O_3	120–140	45–52	5	0.6–1.4
VHS tape	CrO_2	110	44–58	3–4	2
	Co-γ-Fe_2O_3	110	52–74	3–4	2
Hi 8 tape	MP	200	120–135	2–3	8
	ME[a]	350	90	0.2	~125
DVC tape	MP	>300	180	0.15	50
	ME[a]	450	135	0.15	~125
1.4 MB floppy	Co-γ-Fe_2O_3	50	50	1	1.4
100–120 MB floppy	MP	160	125	0.3	8
Data cartridge	MP	200	160	0.2–1.0	20

[a] Denotes intrinsic properties.
[b] Particle density.

done in magnetometers—leads to a rotation of the internal field whose magnitude depends on the tape magnetization itself. Figure 8 illustrates the complex process. The sketches in the upper row indicate some points on the magnetization curve. The middle row roughly indicates the magnitudes and the orientations of the external field, the demagnetizing field, and the internal field for the three points. In order to make a fair comparison between particulate media and ME tape, the direction of the internal field needs to be held fixed. The bottom row in Fig. 8 indicates that the sample has to rotate *during* the measurement of the hysteresis loop. In Fig. 8, the direction of the internal field is held fixed along the longitudinal direction; the little flags indicate the orientation of the film for the three points. Bernards et al. (24) and Richter (13) have measured compensated hysteresis loops of ME tape. These measurements show that the 'intrinsic' hysteresis loop of ME tape is almost perfectly square, with a squareness larger than 0.9 and an SFD smaller than 0.1.

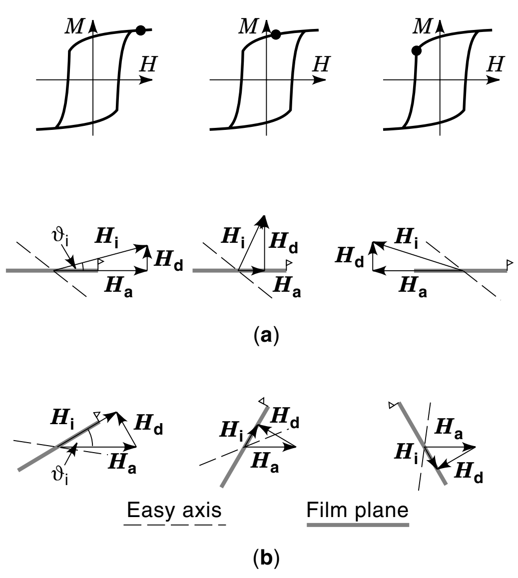

Figure 8. Compensation for demagnetization for metal evaporated tape. *Top row:* points on the hysteresis curve; *middle row:* external field, $\boldsymbol{H}_a$, demagnetizing field, $\boldsymbol{H}_d$, and internal field, $\boldsymbol{H}_i$, for a standard hysteresis measurement; *bottom row:* external field, demagnetizing field, and internal field for a compensated hysteresis measurement. A proper compensation for demagnetization forces the internal field to stay on the same axis during hysteresis measurement.

The compensated measurement shows symmetry around the easy axis as one expects from a magnetically uniaxial material. The 'intrinsic' easy axis forms an angle of 35° to 40° with the film plane. The angle dependence of the switching field, that is, remanent coercivity, is consistent with an incoherent magnetization process. The switching field is lowest along the easy axis and highest perpendicular to the easy axis with value close to the anisotropy field. Uncompensated measurements are not symmetrical, because the demagnetizing field distorts the magnitude and the direction of the internal field as outlined above. Further data show that ME tape is extremely well oriented, with an orientation ratio of about 10.

MAGNETIZATION REVERSAL OF FINE PARTICLES

A magnetic recording medium must consist of a magnetic material with a high enough coercivity to have sufficient safety margin against unwanted erasure. External as well as internal fields (demagnetization) can cause unwanted erasure. The information storage should use as little space as possible. Single-domain particles, that is, magnetic particles that are so small that they cannot break up into a multidomain structure, are consequently best suited for magnetic recording applications. All particles used in recording have uniaxial magnetic anisotropy. Magnetic particles with multiaxial anisotropy were also under discussion (1,25), but did not gain practical importance. To better understand the magnetic recording process, the fundamental switching behavior of single-domain particles is thus of primary interest.

Stoner–Wohlfarth Model (Coherent Rotation)

Stoner and Wohlfarth introduced a simple model for magnetization reversal in single-domain particles in 1948 (26). They assumed that the magnetization in these particles is always homogenous (model of coherent rotation). The model thus applies to elliptical particles only. Initially, it was argued that the strong (but short-ranged) exchange forces are strong

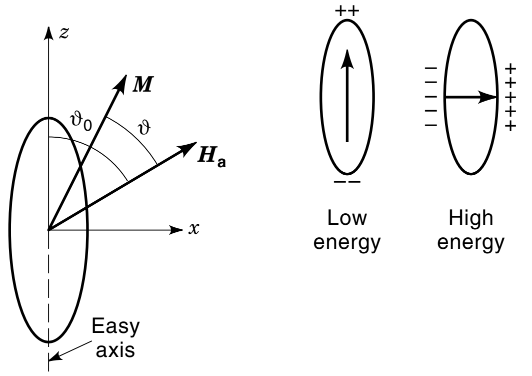

Figure 9. System of coordinates. In the state of lowest magnetostatic energy the magnetic poles are separated as much as possible.

enough to always ensure a homogeneous magnetization. In order to show a hysteresis, the magnetic material must have a magnetic anisotropy. In case of *shape anisotropy,* the magnetization of a single-domain particle seeks to orient itself such that it minimizes magnetostatic energy. As Fig. 9 illustrates, this occurs when the magnetic poles are separated as much as possible. In case of *magnetocrystalline anisotropy,* the crystal itself energetically favors certain magnetization orientations. As an example, consider a material with a hexagonal elementary cell such as cobalt. The *c*-axis of the elementary cell, which is the direction perpendicular to the hexagonal base plane, distinguishes itself from the directions in the base plane. For the particular case of cobalt, the *c*-axis is 'magnetically easy' and the magnetization likes to point along the easy axis.

For a Stoner–Wohlfarth particle with uniaxial anisotropy, the magnetic energy is:

$$E(\vartheta) = -\mu_0 M_s H_a V \cos\vartheta + \frac{1}{2}\mu_0 M_s H'_A V \sin^2(\vartheta - \vartheta_0) \qquad (7)$$

Figure 9 illustrates the angle definitions. ϑ is the angle between the magnetization and the applied field, H_a, and ϑ_0 is the angle between the easy axis and the applied field. In Eq. (7), μ_0 is the permeability of free space, $4\pi\ 10^{-7}$ V·s/A·m, M_s is the saturation magnetization, H'_A is the effective anisotropy field, and V is the volume of the particle. The effective anisotropy field H'_A takes both the shape and the magnetocrystalline anisotropy into account:

$$H'_A = H_A + (N_\perp - N_\parallel)M_s \qquad (8)$$

Here, H_A is the magnetocrystalline anisotropy field, and $N_\perp$ and $N_\parallel$ are the demagnetization factors perpendicular and parallel to the easy axis, respectively. Equation (8) assumes that the two easy axes coincide. In addition, Eq. (8) assumes that the shape of the specimen is an ellipsoid of revolution. In this case, the relation $N_\parallel + 2N_\perp = 1$ holds. Often the anisotropy constant, K_1, is used to describe the magnetocrystalline anisotropy energy. The anisotropy field, H_A, relates to K_1, as follows:

$$H_A = \frac{2K_1}{\mu_0 M_s} \qquad (9)$$

Conceptually, the anisotropy field can be understood as a fictitious field that pulls the magnetization towards the easy axis.

The evaluation of Eq. (7) predicts magnetic hysteresis. The free parameter is the angle of the magnetization, ϑ. Figure 10 shows the energy according to Eq. (7) as function of ϑ. It is convenient to normalize Eq. (7) to $\mu_0 M_s H'_A V$ and to write:

$$h = \frac{H_a}{H'_A} \qquad (10)$$

Depending on the field h, there can be either one or two energy minima (see Fig. 10). If there are two energy minima, two values for the magnetization can be assigned to one field value, that is, there is hysteresis. For higher field magnitudes, Fig. 10 illustrates that one of the minima becomes shallower until it disappears completely. At this point, the magnetization will switch irreversibly to the other energy minimum. Finding the energy minima of Eq. (7) thus determines the hysteresis loop. A necessary condition for an energy minimum is $dE/d\vartheta = 0$, which reads in normalized form:

$$2h\sin\vartheta + \sin[2(\vartheta - \vartheta_0)] = 0 \qquad (11)$$

The stability of the magnetic state requires that $d^2E/d\vartheta^2 > 0$, which reads:

$$2h\cos\vartheta + 2\cos[2(\vartheta - \vartheta_0)] > 0 \qquad (12)$$

The solution of Eq. (11) is not analytical, with the exceptions of the special cases $\vartheta_0 = 0°$ (easy axis parallel to the field), $\vartheta_0 = 90°$ (easy axis perpendicular to the field), and $\vartheta_0 = 45°$. Figure 11 shows the result for $\vartheta_0 = 0°$ and $\vartheta_0 = 90°$. For $\vartheta_0 = 0°$, starting from positive saturation, the magnetization remains on the easy axis until the applied field reaches the critical value. Then the magnetization reverses irreversibly to the opposite direction. The Stoner–Wohlfarth model predicts that the coercivity is equal to the effective anisotropy field. For the case $\vartheta_0 = 90°$ there are only reversible, that is, rotational, processes. For the intermediate cases $0° < \vartheta_0 < 90°$, the magnetization reversal process consists of both reversible and irreversible processes. There is an important difference between the switching field, h_s, and the coercivity, h_c. The coercivity is defined to be the magnetic field at which the projection of the magnetization on the field axis is zero. The

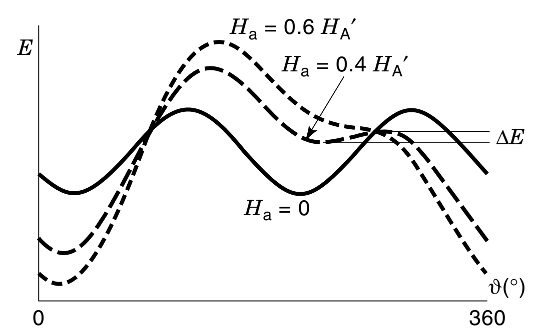

Figure 10. Magnetic energy for a single-domain particle as function of magnetization angle with the field, ϑ. Depending on the field H_a, there can be one or two energy minima. The energy barrier ΔE is required to switch the magnetization.

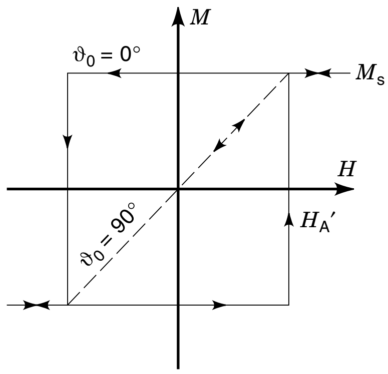

Figure 11. Magnetization reversal by coherent rotation in a single-domain particle: Hysteresis loops for the two cases easy axis aligned with the field ($\vartheta_0 = 0°$) and easy axis perpendicular to the field ($\vartheta_0 = 90°$).

switching field, or remanent coercivity, is the field at which the magnetization switches irreversibly. The coercivity can be equal or less than the switching field.

The magnetic recording process is vectorial in nature. Therefore, the angle dependence of the switching field is of importance. For the case of the Stoner–Wohlfarth model, the angle dependence of the switching field is:

$$h_s(\vartheta_0) = -\frac{1}{(\cos^{2/3}\vartheta_0 + \sin^{2/3}\vartheta_0)^{3/2}} \qquad (13)$$

The negative prefix indicates that the switching occurs at negative field after the sample has been saturated in positive direction. The angle of the magnetization ϑ_c, with respect to the field axis just before switching, is:

$$\vartheta_c(\vartheta_0) = \vartheta_0 + \arctan\sqrt[3]{\tan\vartheta_0} \qquad (14)$$

Real recording media consist of ensembles of single-domain particles. Therefore, the hysteresis loop of an ensemble is an average of the individual loops. For the case of a random distribution of the easy axes, the remanent magnetization is 0.5 M_s and the coercivity is $h_c = H_a/H'_A = 0.48$. This calculation assumes that there exists no magnetic interaction between the particles.

Chain of Spheres (Fanning)

While the Stoner–Wohlfarth model provides a good understanding of basic hysteresis phenomena, the predicted values for the switching fields are too high. The magnetization can also switch inhomogeneously. Rather than modeling elongated recording particles as prolate spheroids, Jacobs and Bean (27) suggested describing the shape anisotropy by a chain of spheres. γ-Fe_2O_3 particles, in particular, have shapes like peanuts. A chain of spheres has a lower shape anisotropy when compared with a prolate spheroid. The shape anisotropy field of a chain of $n \geq 2$ spheres is:

$$H_A^{\text{shape}} = \frac{M_s}{4} K_n \qquad (15)$$

where

$$K_n = \sum_{j=1}^{n} \frac{n-j}{nj^3}$$

Jacobs and Bean discovered that the magnetization reversal is considerably facilitated if the magnetization vectors of adjacent spheres fan out rather than remaining parallel. Figure 12 illustrates that the additional magnetostatic energy partially cancels at magnetization reversal. This means that there is less resistance for the magnetization to overcome at reversal, making the magnitude of the switching field smaller.

As a simplification, the magnetization vectors are often assumed to fan out symmetrically. The switching field of *symmetric fanning* in a chain of n spheres ($n \geq 2$), with additional magnetocrystalline anisotropy along the chain axis, can be calculated analytically:

$$h_s(\vartheta_0) = \frac{1 - f_n}{f_n\sqrt{1 - f_n(2 - f_n)\sin^2\vartheta_0}} \quad \text{for} \quad \vartheta_0 \leq \arctan\left(\frac{1}{(f_n - 1)^{3/2}}\right) \qquad (16)$$

where

$$f_n = \frac{3}{2}\frac{K_n + 4/\omega}{L_n}$$

$$L_n = \sum_{j=1}^{1/2(n-1)<j<1/2(n+1)} \frac{n - (2j - 1)}{n(2j - 1)^3}$$

The parameter ω is proportional to the ratio between magnetocrystalline and shape anisotropy energy:

$$\omega = \frac{\frac{1}{2}\mu_0 M_s^2}{\frac{1}{2}\mu_0 M_s H_A} = \frac{M_s}{H_A} \qquad (17)$$

For an infinitely long chain of spheres, Fig. 12 gives the result for the switching field as function of field angle. The switching field is normalized to its effective value, that is, the sum of the magnetocrystalline and shape anisotropy field. For dominating shape anisotropy, $\omega \to \infty$, the switching field is considerably reduced, especially for small angles ϑ_0 between the

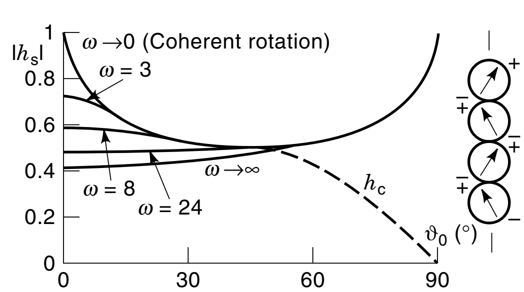

Figure 12. Reduced switching field ($h_s = H_s/H'_A$) as function of angle between applied field and easy axis, ϑ_0, for the fanning mechanism. In case of coherent rotation, the magnetization remains parallel, while they fan out otherwise. Increasing magnetocrystalline anisotropy ($\omega = M_s/H_A$) drives the reversal mechanism back to coherent rotation.

field and the easy axis. At larger angles ϑ_0, the fanning procedure does no longer efficiently lower the energy barrier for the magnetization reversal. Then the Stoner–Wohlfarth process (parallel magnetization vectors of the spheres) takes over. For strong magnetocrystalline anisotropy, $\omega \to 0$, the contribution of the shape anisotropy field to the total anisotropy field is small and the switching fields approach those of coherent rotation.

The chain-of-spheres model and variations thereof have been discussed in various papers, for example (28). It was noted that the magnetization inside these spheres does not remain homogenous as assumed before (29).

Nucleation Theory

While the fanning model successfully describes an inhomogenous magnetization reversal process, it still fails to predict the size dependence of the switching field of fine particles. Using a micromagnetic approach, Brown (30) and Frei et al. (31) obtained more realistic switching fields than those predicted by Stoner and Wohlfarth. Micromagnetic theory works on a scale that is small enough to describe magnetization distributions in ferromagnetic bodies with sufficient accuracy, but large enough to replace the individual spins by a continuous magnetization (32–34). The total magnetic energy E of the particle is composed of exchange energy, magnetocrystalline energy, field energy, and magnetostatic energy:

$$E = \iiint \left\{ A[\nabla m_x)^2 + (\nabla m_y)^2 + (\nabla m_z)^2] + e_c - \mu_0 \boldsymbol{M} \cdot \boldsymbol{H}_a - \frac{1}{2}\mu_0 \boldsymbol{M} \cdot \boldsymbol{H}_d \right\} dV \tag{18}$$

where

A = exchange constant
m_i = direction cosines of the magnetization
e_c = magnetocrystalline anisotropy energy density
$\boldsymbol{H}_d$ = demagnetizing field
ΔV = volume element

Starting again with an ellipsoidal particle magnetized homogeneously by application of a very large positive field, the field is lowered slowly (in order to avoid dynamic effects) and, if required, reversed until the magnetization switches irreversibly. As long as the magnetization has not switched irreversibly, the equilibrium angle ϑ of the magnetization is still given by solving Eq. (11). The next step is to allow a small deviation from that equilibrium state (since any magnetization reversal must begin with a small change) and determine the total energy change associated with that deviation. It is important to allow the magnetization to leave its equilibrium state in an arbitrary manner, in order to find the *mode* that facilitates magnetization reversal the most. Mathematically, this corresponds to a linearization of the particle's magnetic energy around the current equilibrium state. The magnetization reversal mode is determined by minimization of the *second*-order energy change (the first-order energy change is zero). For the case discussed here, this energy change is

$$\Delta E^{(2)} = \iiint \{[(\nabla\xi)^2 + \lambda_\xi \xi]\epsilon^2 + [(\nabla\eta)^2 + \lambda_\eta \eta]\epsilon^2\} dV \tag{19}$$

Here, $\xi = \xi(x, y, z)$ and $\eta = \eta(x, y, z)$ are test functions, ϵ is a small quantity and the factors λ_ξ and λ_η have to be determined from the total energy. Applying a standard variational procedure to Eq. (19) leads to a set of differential equations known as *Brown's equations.* Any nontrivial solution of these equations indicates that either the state of homogeneous magnetization can be left or that coherent rotation occurs (Stoner–Wohlfarth switching). The largest external field strength at which this can happen is the *nucleation field.*

The most important nonuniform reversal process is the *curling* mode. When the magnetization leaves the uniform state, curling creates no additional poles in the plane perpendicular to the magnetization (see Fig. 13). This happens at the expense of exchange energy. Since the exchange energy is very strong and has a very short range, while the magnetostatic energy is weaker, but has a long range, the particle size has a strong influence on the nucleation field, H_n:

$$H_n = -H_A - \frac{k_c M_s}{2S^2} + N_\parallel M_s \tag{20}$$

where

$$S = \frac{R}{R_0}$$
$$R_0 = \frac{1}{M_s}\sqrt{\frac{4\pi A}{\mu_0}}$$

Here S is a reduced radius and k_c depends on the aspect ratio of the ellipsoid of revolution. The factor k_c varies between 1.08 (infinite cylinder) and 1.42 (very thin plate) (35,36). If the magnitude of the second term exceeds $N_\parallel M_s$, coherent rotation takes over. Equation (20) holds for alignment of both anisotropy axes with the external field.

The Euler–Lagrange equations deduced from Eq. (19) cannot be solved analytically for $\vartheta_0 \neq 0$ and $e_c \neq 0$. There is no curling in this case, because the magnetocrystalline anisotropy breaks the symmetry for $\vartheta_0 \neq 0$. Omitting the energy associated with the creation of additional poles at the beginning of magnetization reversal (which is strictly true only for curling), the following equation gives an upper bound for H_n (37):

$$H_n \cos\vartheta + H_A \cos 2(\vartheta - \vartheta_0) - M_s[N_\parallel \cos^2(\vartheta - \vartheta_0) + N_\perp \sin^2(\vartheta - \vartheta_0)] + \frac{k_c M_s}{2S^2} = 0 \tag{21}$$

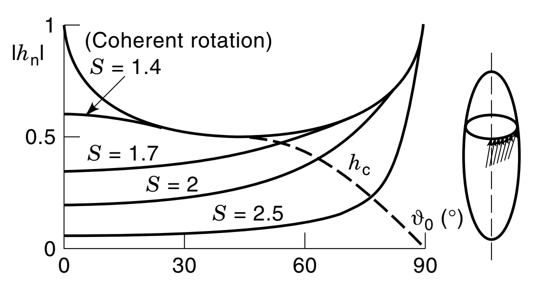

Figure 13. Reduced curling nucleation field ($h_n = H_n/H'_A$) for a prolate spheroid with aspect ratio 4 as function of angle between applied field and easy axis, ϑ_0. For small particle radius, S, the nucleation fields increase until they approach those for coherent rotation. No additional magnetic poles are created at curling.

Figure 13 shows the normalized nucleation fields as a function of field angle for elongated ellipsoidal particles for $e_c = 0$ (aspect ratio: 4). Similar as for fanning, increasing magnetocrystalline anisotropy drives the nucleation fields back to the Stoner-Wohlfarth solution. Figure 13 also shows that the switching fields of curling approach those of coherent rotation for small radius S. The general shapes of the angle dependence of the switching field of curling and fanning are similar (see Figs. 12 and 13). There exists always a reduced radius S which makes the curling solution agree with that of fanning. Therefore, a measurement of the angle dependence of the switching or the coercive field cannot identify the magnetization reversal mechanism.

In addition to rotation in unison and curling, *magnetization buckling* is another solution of Brown's equations for an infinite cylinder. Magnetization buckling is similar to the fanning mechanism. This mode introduces only very small changes in nucleation field, compared with the other two modes (31). It is of no practical interest, since it cannot occur in prolate spheroids of reasonable aspect ratio (38). In recent years, magnetization reversal has extensively been studied numerically; Schabes gives a review (39). Generally, the numerical calculations indicate that magnetization reversal starts at one end of the particle. The reader can obtain information on classical nucleation theory in (32–34,36,40,41).

Thermally Activated Magnetization Reversal Processes

For high-density recording, the particles in a recording medium should be as small as possible. As will be discussed in the section "Recording Physics," small particles lower the medium noise and potentially allow for smoother tape surfaces. On the other hand, extremely small particles—although magnetically ordered—lose their hysteresis. As shown in Fig. 10, stable magnetization states have local energy minima that are separated by energy barriers. If thermal energy can overcome these energy barriers, the critical fields discussed above will no longer be valid. In a noninteracting particle assembly with identical energy barriers, $\Delta E(h)$, for each particle, virtually any theory leads to (42):

$$\nu_{1,2} = f_0 \exp\left(-\frac{\Delta E(h)}{k_B T}\right) \tag{22}$$

where

$k_B = 1.38 \times 10^{-23}$ J/K (Boltzmann's constant)
T = temperature in K
f_0 = "attempt" frequency

In Eq. (22) $\nu_{1,2}$ is the probability for one particle to switch from the magnetization state 1 to state 2 in the time interval dt. Within the model of coherent rotation, the energy barrier is identical to the particle volume. For very small particle volumes, $\nu_{1,2}$ will be so large that a particle assembly cannot remain magnetized after removal of a field (superparamagnetism). However, a stable remanence is not the criterion for a lower limit of particle size for recording media. The thermal energy seeks to completely randomize a magnetic system. The longer the time interval in which the thermal forces can operate, the more attempts they can make to successfully demagnetize the system. Similarly, if a magnetic field is applied, the thermal forces will assist to switch the magnetization. For an assembly of Stoner–Wohlfarth particles with their easy axes aligned with the field, the energy barrier depends on the normalized field $h = H_a/H'_A$ as follows:

$$\Delta E(h) = \frac{1}{2}\mu_0 M_s H'_A V(1+h)^2 = \Delta E_0(1+h)^2 \tag{23}$$

The time-dependent switching field can be calculated (43,44):

$$|H_s(t)| = H'_A \left\{1 - \sqrt{\frac{k_B T}{\Delta E_0} \ln\left(\frac{f_0 t}{\ln 2}\right)}\right\} \tag{24}$$

Equation (24) imposes a practical limit on the minimum particle size useful for magnetic recording. Figure 14 shows some curves for the normalized switching field as a function of time. The height of the energy barrier ΔE_0 is varied and given in multiples of $k_B T$. For small values ΔE_0, the difference between the long-term coercivity, or "storage coercivity," and the short-term coercivity, or "writing coercivity" becomes large. A difference of about factor of two between the two coercivities may be tolerable.

Experimental data on the time dependence of the switching field follow the theoretical curves predicted by Eq. (24) well over many orders of magnitude (45). For very short times, the switching field increases sharply (46). This may indicate that Eq. (24) is no longer valid because the pulse length approaches $1/f_0$. Unfortunately, little is known about the escape frequency f_0. Brown gave an estimate in 1963 (47):

$$f_0 = \frac{\mu_0|\gamma|H'_A\alpha}{1+\alpha^2}\sqrt{\frac{\mu_0 M_s H'_A V}{2\pi kT}}(1-h^2)(1+h) \tag{25}$$

In Eq. (25), $\gamma = -1.761\ 10^{11}$ 1/Ts is the gyromagnetic ratio, and α is the damping constant. Typical data for recording media yield 10^9 Hz for the order of magnitude for f_0. Using Mößbauer measurements a value of 10^{12} Hz has been reported (48), but the switching data fit better if the value of f_0 is 10^9 Hz (46). The reasonable agreement between theory and experiment is presumably fortuitous. It is well established that

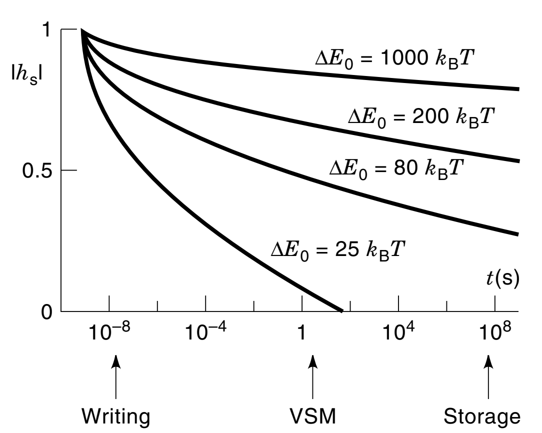

Figure 14. Reduced switching field ($h_s = H_s/H'_A$) as function of time scale for coherent rotation. The magnetic energy barrier at zero field, ΔE_0, is given in multiples of $k_B T$. For small energy barriers, the thermal energy reduces stability, which introduces a time-dependent coercivity.

magnetic recording particles do *not* reverse their magnetization coherently and the assumptions leading to Eq. (24) are therefore not valid. Equation (24) is not even valid for the Stoner–Wohlfarth model, since the field dependence of the energy barrier, Eq. (23) does not hold for arbitrary ϑ_0. A theoretical argument by Victora suggests that the exponent of 2 in Eq. (23) should be replaced by 1.5 (49).

An alternative approach to analyze thermally activated magnetization processes is the concept of a fluctuation field (50). The fluctuation field is best defined by equating two energies, namely, the thermal energy, k_BT, and the Zeeman energy of the magnetic moment M_sV_A in a fictitious fluctuation field, H_F:

$$H_F = \frac{k_BT}{\mu_0 M_s V_A} \tag{26}$$

Here V_A is the *activation volume.* Street and Woolley introduced time-dependent magnetization measurements (*magnetic viscosity*), which serve to determine fluctuation fields and activation volumes (51). For a Stoner–Wohlfarth particle, one expects the activation volume to be proportional to the particle volume. In most cases, fine magnetic particles have activation volumes smaller than the particle volume. The interpretation is that only a small portion of the particle is 'thermally activated' in the first instance. Once the small volume reverses magnetization, the rest of the particle follows. Using magnetic viscosity measurements, the fluctuation field of CrO_2 was found to be larger than that of Co doped γ-Fe_2O_3 (52). This is presumably due to the lower Curie temperature of CrO_2. Because of this large magnetic viscosity, CrO_2 tapes with lower nominal coercivity turn out to be equivalent in recording to their counterparts based on Co doped γ-Fe_2O_3. Magnetic viscosity measurements were also applied to standard and advanced MP and showed that, contrary to the expectation, the bigger particles were magnetically less stable than the smaller ones (53). The structure of the particles explains this result: the larger particles contain more (and smaller) crystal grains, which probably are the relevant units for magnetization reversal. For further study, the reader is referred to Refs. 42, 47, 50.

Print-through. A practical consequence of thermal activation is *print-through* (PT), which occurs in analog audio systems (1,54). PT is the unwanted copying of the recorded signal onto neighboring layers in the tape reel. Because of spacing and thickness loss factors, the wavelength with the maximum printing field is $2\pi t$, where t is the total tape thickness. For audiocassettes, this corresponds to a frequency of approximately 650 Hz. PT leads to audible echoes or even more disturbing foretastes of coming load passages. Since the human ear is sensitive to PT levels lower than −50 dB, only a small fraction of the particles need to have a small enough activation volume to be susceptible to the printing field.

Using larger particles reduces PT, but leads to an increased particle noise. Therefore, tightening the particle size distribution is a measure to improve PT. Another approach has been double-layer coating: the top layer uses finer particles for good noise performance, while the bottom layer uses larger particles to reduce PT. Digital systems, which are the only new systems being introduced, use only short wavelengths (less than a few micrometers). Then the spacing loss attenuates the stray fields and PT is not a problem.

RECORDING PHYSICS

When information is recorded magnetically on a tape, the recording head imprints magnetic patterns onto the medium. The magnetic layer of the tape serves to retain these patterns and to provide some means to retrieve the information. The stray field outside the tape reflects the magnetization of the tape and can thus be used for information retrieval. Since the field lines of the magnetic flux density must be closed, there is a magnetic field inside the magnetic material as well. This field—the demagnetizing field—opposes the magnetization. Since the demagnetizing field seeks to destabilize its own source, there has always been concern that excessive demagnetization may eventually destroy the recorded magnetization pattern. For tape recording, it is current understanding that, in particular, geometrical effects strongly influence the written magnetization patterns, which makes the question of demagnetization far less critical than initially thought.

Magnetic Recording Principle

Figure 15 sketches the basic recording principle. For writing information, a current is fed into the *recording head,* which moves relatively to the medium. Depending on the current direction, the stray field of the head switches the magnetization to the left or to the right. In case of digital recording, one always wishes to magnetize the medium up to saturation. Between the regions of saturated magnetization, there are *magnetization transitions.* For achieving a high recording density, the width of these transitions has to be kept as small as possible. The number of transitions (or flux changes) per length is the *linear density.*

Information is stored in digital magnetic recording by changing the distance between transitions. Since there is a clock in every digital system, the transitions are always separated by multiples of

$$B = vT_0 \tag{27}$$

where T_0 is the clock period and v is the head to medium velocity. Although not strictly correct, it is customary to call B the *bitlength.* Squarewave recording is used to study the fundamental recording behavior of heads and media. In this

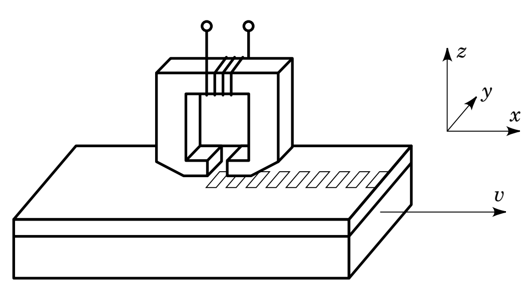

Figure 15. Recording principle and definition of the coordinate system. When the energized recording head is moved relatively to the medium, a magnetization pattern can be written onto the medium. Where the recorded medium is passed over the readback head, a readback voltage is induced.

case, the spacing between transitions is constant and one defines a wavelength λ as

$$\lambda = 2B \tag{28}$$

Typically, the width of the track is much wider than the transition spacing and the medium thickness. Therefore, track width dependencies are often neglected and the magnetic recording process becomes two-dimensional.

The magnetic flux, ϕ, emanating from the medium, is used to retrieve the written information. In case of inductive reading, any change of the stray flux that is sensed by the readback head, ψ, leads to an induced voltage:

$$\text{emf} = -w\,\frac{d\psi}{dt} \tag{29}$$

Here w is the number of turns. Many recording systems use the same head for reading and writing. Magnetoresistive readback provides higher output voltages than inductive reading. While the bulk of the tape systems still use inductive readout, most of the newly introduced systems use a magnetoresistive transducer.

The recording principle for *perpendicular* recording is the same as that for longitudinal recording. The recording head shown in Fig. 15 is also termed *ring head.* Although a ring head can record on perpendicular media, it is more effective to use its magnetic counterpart, a *single-pole head.* The true magnetic counterpart to the ring head would be a single-pole head without a flux return path (55), but the efficiency of this structure is virtually zero. A magnetically soft layer underneath the recording layer provides a part of the required flux return path. This underlayer belongs magnetically to the head and physically to the medium. Such an underlayer has to be relatively thick [several times the thickness of the recording layer (22)] to prevent saturation at longer wavelengths. Unfortunately, the additional underlayer creates noise (56). ME tape has an easy axis tilted out of the film plane and is thus in between longitudinal and perpendicular media, but is identified as a longitudinal medium.

The recording process is most conveniently studied on a macroscopic scale, because a detailed discussion of the relevant magnetization processes on a micromagnetic level is too complicated. Even on a macroscopic scale, theoretical recording simulations require extensive computational efforts. For many purposes, simplified models are more appropriate than the more complex numerical models.

Magnetization and Demagnetizing Fields

In digital magnetic recording, the magnetization of a medium consists of magnetically saturated regions separated by magnetization transitions. The direction of the magnetization in neighboring "bits" points in opposite directions. Continuous magnetization distributions—which is a reasonable assumption if the particle size is much smaller than the bit pattern—create demagnetizing fields that can be calculated from:

$$\boldsymbol{H}_\text{d} = -\frac{1}{4\pi}\iiint\limits_\text{volume}\frac{\nabla'\cdot\boldsymbol{M}'(\boldsymbol{r}')(\boldsymbol{r}-\boldsymbol{r}')}{|\boldsymbol{r}-\boldsymbol{r}'|^3}\,dV' + \frac{1}{4\pi}\iint\limits_\text{surface}\frac{\boldsymbol{n}'\cdot\boldsymbol{M}(\boldsymbol{r}')(\boldsymbol{r}-\boldsymbol{r}')}{|\boldsymbol{r}-\boldsymbol{r}'|^3}\,dA' \tag{30}$$

Here the first expression gives the field due to volume charges $\rho_m = -\nabla\cdot\boldsymbol{M}$ and the second term that due to surface charges $\sigma_m = \boldsymbol{n}\cdot\boldsymbol{M}$, where $\boldsymbol{n}$ is a normal vector. For some special magnetization patterns, Eq. (30) can be evaluated analytically. For a tape of thickness δ and infinite width in the direction across the track, the volume charges correspond to a longitudinal magnetization M^L and the surface charges to a vertical magnetization M^V. Therefore, it is favorable to split Eq. (30) into longitudinal and vertical magnetization components. A sinusoidally magnetized tape with a constant magnetization through its depth (z-direction) creates sinusoidal demagnetizing fields in x- as well as in z-direction. Outside the tape, the stray flux (and the stray field) decays exponentially with distance (57,58):

$$\phi = \phi_0\exp(-kz) \tag{31}$$

Here k is the wavenumber, $k = 2\pi/\lambda$. Eq. (31) is a direct consequence of the Laplace equation in two dimensions. Equation (31) can be converted to yield -54.6 dB z/λ. This *spacing loss* is the most important single factor for designing a recording system.

The decay of the stray flux in Eq. (31) does not depend on the orientation of the magnetization. Thus, there is no difference in stray field magnitude for longitudinal and perpendicular recording. If the tape magnetization rotates by an angle θ_0, the stray fields rotate by $-\theta_0$, (59). The fields *inside* the medium depend on the orientation of the magnetization and are evaluated here for two planes, $z' = 0$ (center plane of the medium) and $z' = \delta/2$ (surface plane of the medium) (55,60):

$$H_{\text{d},x} = -M^\text{L}\begin{cases}1-\exp\left(-\dfrac{k\delta}{2}\right) & \text{for } z'=0\\[2mm] \dfrac{1}{2}\,[1-\exp(-k\delta)] & \text{for } z'=\dfrac{\delta}{2}\end{cases} \tag{32}$$

$$H_{\text{d},z} = -M^\text{V}\begin{cases}\exp\left(-\dfrac{k\delta}{2}\right) & \text{for } z'=0\\[2mm] \dfrac{1}{2}\,[1+\exp(-k\delta)] & \text{for } z'=\dfrac{\delta}{2}\end{cases} \tag{33}$$

The primes indicate that the coordinate system is attached to the medium. Unprimed quantities will be used for the head system. If only the center plane of the medium, $z' = 0$, is considered, perpendicular recording seems to be much more favorable. When the recording density is increased, demagnetization increases for longitudinal recording, while it decreases for perpendicular recording. On the other hand, the demagnetizing field at high density always approaches 50% of the magnetization *at the medium surface.* This means that the external fields—which account for the reading signal—are not necessarily expected to be larger for perpendicular recording. A potential demagnetization advantage of perpendicular recording requires that the product $k\delta$ is large enough. In practice, perpendicular media must remain writable, which limits δ and, therefore, the product $k\delta$ (56). The presence of a soft magnetic underlayer does not change these conclusions (61).

Another useful field configuration that can be calculated analytically is an arctan-like magnetization transition. There is no physical justification for assuming that the transition shape is exactly like an arctan, but this approach has been widely used because of mathematical convenience:

$$M(x') = -\frac{2M}{\pi}\arctan\frac{x'}{a} \qquad (34)$$

Here, a is the *transition parameter,* which describes the transition sharpness. Equation (34) assumes that the magnetization transition does not change as a function of depth, that is, it is valid for thin media.

Several analyses have shown that the arctan transition has too long tails. The hyperbolic tangent or the error function more realistically describes the shape of a magnetization transition. Evaluation of Eq. (30) with Eq. (34) yields for the longitudinal demagnetizing field due to the longitudinal magnetization:

$$H^{\mathrm{L}}_{\mathrm{d},x}(x',z') = \frac{M^{\mathrm{L}}}{\pi}\left\{\arctan\left(\frac{x'\left(\frac{\delta}{2}+z'\right)}{x'^2+a^2+\left|\frac{\delta}{2}+z'\right|a}\right) + \arctan\left(\frac{x'\left(\frac{\delta}{2}-z'\right)}{x'^2+a^2+\left|\frac{\delta}{2}-z'\right|a}\right)\right\} \qquad (35)$$

The perpendicular demagnetizing field of the magnetization transition $M_x(x')$ is:

$$H^{\mathrm{L}}_{\mathrm{d},z}(x',z') = \frac{M^{\mathrm{L}}}{2\pi}\ln\left[\frac{x'^2+\left(a+\left|\frac{\delta}{2}+z'\right|\right)^2}{x'^2+\left(a+\left|\frac{\delta}{2}-z'\right|\right)^2}\right] \qquad (36)$$

For a vertical magnetization transition:

$$M_z(x') = -\frac{2M^{\mathrm{V}}}{\pi}\arctan\frac{x'}{a} \qquad (37)$$

One obtains for the vertical demagnetizing field:

$$H^{\mathrm{V}}_{\mathrm{d}}(x',z') = \frac{M^{\mathrm{V}}}{\pi}\left\{\mathrm{sgn}\left(\frac{\delta}{2}+z'\right)\arctan\left[\frac{x'}{a+\left|\frac{\delta}{2}+z'\right|}\right] + \mathrm{sgn}\left(\frac{\delta}{2}-z'\right)\arctan\left[\frac{x'}{a+\left|\frac{\delta}{2}-z'\right|}\right]\right\} \qquad (38)$$

The functional dependence of the longitudinal demagnetization field due to the vertical magnetization component is $H^{\mathrm{V}}_{\mathrm{d},x}/M^{\mathrm{V}} = -H^{\mathrm{L}}_{\mathrm{d},z}/M^{\mathrm{L}}$.

For a longitudinal magnetization transition, the demagnetization fields are strongest at some distance to the middle of the transition. For $M^{\mathrm{L}} > H_{\mathrm{c}}$, a perfectly sharp transition cannot occur because the demagnetizing fields will exceed coercivity and the transition must broaden. This imposes a limit on the transition parameter a (*demagnetization limit*). The demagnetization limit is of little practical importance. As outlined in the next section, typically, the transition length determined by the writing process itself is already larger than that imposed by the demagnetization limit.

For pure vertical magnetization, the strongest demagnetization occurs 'in the bit' which limits M^{V} to the coercivity. Since demagnetization does not hinder the vertical magnetization change at the transition, the magnetization can, in principle, increase up to its saturation value when the transition center is approached. From the considerations on sinusoidal magnetization, it follows, however, that the surface demagnetization fields limit the magnetization near the surface to $M_{\max} = 2H_{\mathrm{c}}$ at close transition spacing.

Readback

The reciprocity principle allows calculating the reading signal from a tape with a known magnetization pattern. The flux linkage ψ between the tape and a head having a field $\boldsymbol{h}_{\mathrm{H}}$ when fed by a unit current is:

$$\psi = \mu_0 \iiint_{\mathrm{medium}} \boldsymbol{M}\cdot\boldsymbol{h}_{\mathrm{H}}\,dV \qquad (39)$$

Good approximations of the ring head fields are the formulas of Karlqvist (62) for distances larger than about 0.2 g from the head gap edges:

$$H_{\mathrm{H},x} = \frac{H_{\mathrm{g}}}{\pi}\left[\arctan\left(\frac{g/2+x}{z}\right)+\arctan\left(\frac{g/2-x}{z}\right)\right] \qquad (40)$$

$$H_{\mathrm{H},z} = \frac{H_{\mathrm{g}}}{2\pi}\ln\left[\frac{(g/2-x)^2+z^2}{(g/2+x)^2+z^2}\right] \qquad (41)$$

Here H_{g} is the deep gap field and g is the gap length. For distances closer to the gap edges, Szczech et al. give analytical formulas (63). Assuming a track width W being large compared with the other dimensions, a sinusoidal magnetization with peak value M_{r} homogeneous throughout the depth of the medium yields an induced voltage:

$$V_{0p} = \mu_0 M_{\mathrm{r}} v\eta w W(1-e^{-k\delta})e^{-kd}\frac{\sin 1.13\,g\cdot k/2}{1.13\,g\cdot k/2} \qquad (42)$$

Here η gives the efficiency of the head, w the number of turns, d the head to medium separation, and v the relative velocity between head and medium. Equation (42) contains the spacing loss (e^{-kd}) discussed previously. Equation (42) also takes into account that the parts of the medium closer to the head suffer less from spacing loss than those, which are further away. If no losses occurred, one would expect that the output voltage is proportional to the medium thickness δ. The integration through the depth of the medium yields that the equivalent thickness δ_{eff} fully contributing to the output is:

$$\delta_{\mathrm{eff}} = \frac{(1-e^{-k\delta})}{k\delta}\,\delta \qquad (43)$$

The ratio $\delta_{\mathrm{eff}}/\delta$ is called *thickness loss.* The name is somewhat misleading, since there is no loss due to the thickness rather than less gain than expected.

The *gap loss* [last term of Eq. (42)] takes into account that the output decreases if the wavelength λ approaches the (read) gap length g. For the Karlqvist approximation, the factor 1.13 in Eq. (42) is missing. This factor or similar ones appear for more accurate modeling of the head field and can be used for $\lambda < g$. The field components $H_{\mathrm{H},x}$ and $H_{\mathrm{H},z}$ form a

Hilbert pair, which means that, after a Fourier transformation, they have identical amplitude spectra, but their phase spectra are shifted by 90°. Note that Eq. (42), as it stands, holds for inductive heads. For magnetoresistive readout, the output signal no longer depends on the linear velocity.

For digital recording, the output of an isolated transition is of interest. Combining Eq. (29) and Eq. (39) for thin media, the induced voltage can be written:

$$V(x) = -\mu_0 v\eta w W\delta \int_{-\infty}^{+\infty} h_H(x'-x)\frac{\partial M(x')}{\partial x'}\,dx' \qquad (44)$$

For a step-like magnetization transition, $a \to 0$ (i.e., dM/dx' is a delta function), Eq. (44) demonstrates that the voltage $V(x)$ simply follows the head field. The magnetization orientation determines whether the shape of the replay pulse samples the longitudinal or the vertical component of the head field, or a mixture thereof. If the transition sharpness is finite, ($a > 0$), the readback pulse is approximately equal to that which would occur if a perfectly sharp transition would be written at spacing $d + a$. The equivalence of head to medium spacing and transition parameter is also seen from the Fourier transform of Eq. (34):

$$\mathscr{M}(k) = \frac{2jM_r}{k}e^{-|k|a} \qquad (45)$$

Here $\mathscr{M}$ indicates the Fourier transform and $j = \sqrt{-1}$. Therefore, the effect of transition sharpness and head to medium spacing cannot be distinguished experimentally. The quantity $d + a$ is also called *generalized spacing.* For further study, the following literature is recommended: (60,61,64–67).

Recording Geometry

The *recording geometry* strongly controls the shape and width of the written transitions. For contact recording, omitting demagnetization is a reasonable assumption (68). Bertram et al. point out that the angle dependencies of the particle switching control the shape of the written transitions (69). It is convenient to plot the head fields in a form $|H_H|$ versus θ rather than using the conventional splitting into longitudinal and vertical field components ($|H_H|$ = magnitude of the head field and θ = angle of the head field with the film plane).

Figure 16 shows a parametric plot of the magnitude of the head field from a ring head. The field is plotted as function of

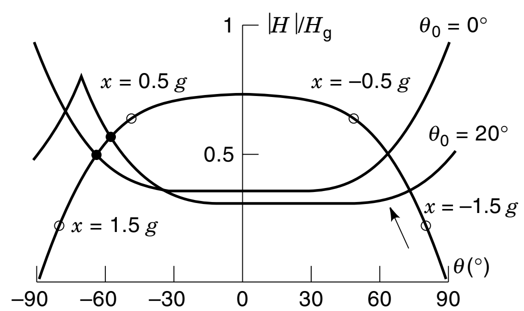

Figure 16. Polar plots: field magnitudes as function of angle. When the medium passes by the head, the field seen by the medium continuously changes magnitude and direction. The open circles indicate the magnitude and direction of the head field for some positions x in units of gap length g. The other two curves labeled $\theta_0 = 0°$ and $\theta_0 = 20°$ represent switching field curves for two different particle orientations. The filled circles indicate where the head field is larger than the medium switching field for the last time (writing location).

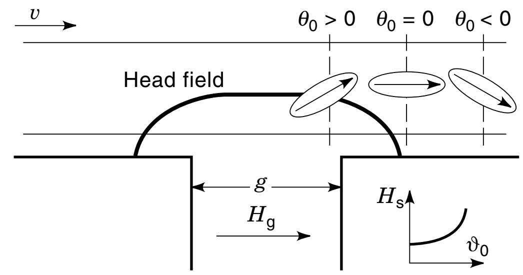

Figure 17. Recording geometry: the interplay between head field and angle dependence of the switching field creates semicircular magnetization patterns at writing.

angle that the tape sees when the head passes by. The hidden parameter is the location x as indicated on the curve. Here the angle $\theta = 0$ corresponds to a field pointing into the longitudinal direction. At large negative values x/g, the head field points into the positive z direction. With increasing x/g, the magnitude of the head field changes (and peaks at the gap edges for small z/g), while the field angle decreases continuously.

For incoherent magnetization processes, the switching field typically increases monotonically with the angle between easy axis and field (see the section titled "Nucleation Theory"). If such a particle is oriented longitudinally, the switching field curve has its lowest point at $\theta = 0$ when plotted into Fig. 16. If the particle is tilted in the xz plane ($\theta_0 > 0$), the switching curve shifts as illustrated in Fig. 16. The cusp for the switching field curve shown in Fig. 16 corresponds to the hard axis location. The state of magnetization "freezes" when the head field becomes smaller than the switching field, which is indicated by the filled circles in the figure. Figure 16 also illustrates the effect of different switching fields. For a larger switching field—which corresponds to a larger value for $h_r = H_r/H_g$—the freezing point will be closer to the gap. Therefore, the SFD has a direct effect on the transition width, even when there is *no demagnetization.* Since nonuniform particle orientations also result in a spread of writing locations, the effect of particle alignment is equivalent to an additional SFD (70).

These geometrical effects have a direct consequence for tape recording. Figure 17 sketches the writing locations for three identical particles with different orientation. The magnetization of each particle is assumed to lie on its easy axis. Evidently, the resulting magnetization forms a semicircular pattern. Tjaden and Leyten observed similar patterns as early as 1964 in a scaled up model system (71). Mallinson has shown theoretically, that a rotating magnetization can create a *one-sided flux* (72), which has double the field intensity on one side and none on the other. Due to the different magnetization directions and writing locations, the external stray fields of one-sided fluxes can either increase or decrease. For small wavelengths, this mechanism predicts nulls in the output curves as function of write current.

Transition Models

A very successful model for longitudinal recording on thin-film media is the *slope model* of Williams and Comstock (67). The main idea is that the head field gradient counterbalances the slope of the demagnetizing field at the center of a transition being written. The original slope model takes only longitudinal components into account, which implies that the medium switching field as function of field angle, H_s, is proportional to $1/\cos\theta$. The slope model discussed in the following is also valid for different angle dependencies of the switching field and easy axis orientations other than longitudinal (73).

The head fields and the mean demagnetizing fields are evaluated at a distance $z = d + \delta/2$ from the head surface (center plane of the medium). The first step is to determine the writing location x_w, which is the center of the magnetization transition being written. The slope of the total magnetization $d|\boldsymbol{M}|/dx$ is:

$$\frac{d|\boldsymbol{M}|}{dx} = \frac{d|\boldsymbol{M}|}{d|\boldsymbol{H}_{tot}|}\frac{d|\boldsymbol{H}_{tot}|}{dx} \tag{46}$$

Assuming a transition shape according to an arctan function one obtains from Eq. (46):

$$\begin{aligned} a = &-\frac{\delta}{4} - \frac{M_r^V \sin\theta_w}{\pi Q} \mp \frac{H_s}{\pi Q}\text{SFD} \\ &\pm \sqrt{\left(\frac{\delta}{4} + \frac{M_r^V \sin\theta_w}{\pi Q}\right)^2 - \frac{M_r^L \delta \cos\theta_w}{\pi Q} \mp \frac{\delta H_s}{\pi Q}\text{SFD}} \end{aligned} \tag{47}$$

where $Q = \cos\theta_w\, dH_{H,x}/dx + \sin\theta_w\, dH_{H,z}/dx$. Here $dH_{H,x}/dx$ and $dH_{H,z}/dx$ give the gradients of the two head field components and θ_w is the field angle at the writing point x_w. The model can be extended to cover the shunting effect of the head by adding the magnetic images, but the solution is no longer analytical. Apart from the effects of magnetization, coercivity, and SFD on the a-parameter in longitudinal recording, the model explains essential features of recording on media with an inclined easy axis (ME tape). At positive θ_0 ($M_r^V > 0$)—easy axis orientation as in the left particle shown in Fig. 17—the model predicts a smaller a-parameter, that is, the transitions are sharper and the output is larger. In this case, a thicker layer can be written with a high field gradient as opposed to the other easy axis inclination. Inspection of Eq. (47) also shows that the perpendicular demagnetizing field narrows the transitions for $\theta_0 > 0$ while it broadens them for $\theta_0 < 0$. For ME tape, the optimum recording occurs when the writing takes place near the magnetically hard axis, that is, at writing the head field is *not* aligned with the easy axis. Typically in the range of an easy axis inclination of $\theta_0 = 20°$ to $50°$, the writing field direction crosses the hard axis, which means that the recorded magnetization changes direction. In such a case, the switching field curve shown in Fig. 16 would shift so far to the right, that the head field would intersect it on the left-hand side from the cusp. Since real ME tape is not perfectly oriented, the recording geometry can lead to double transitions, which means that there are two freezing points rather than one. One can also say that the trailing edge of the head can no longer overwrite entirely what the leading edge has written. These kinds of double transitions also occur in perpendicular media when written with a ring head (73).

Another type of writing interference occurs in isotropic media at low writing currents (25). In this case, the leading edge and the trailing edge of the head both record on the medium. The field at the trailing edge does not fully overwrite the recording of the leading edge any more (geometrical reasons

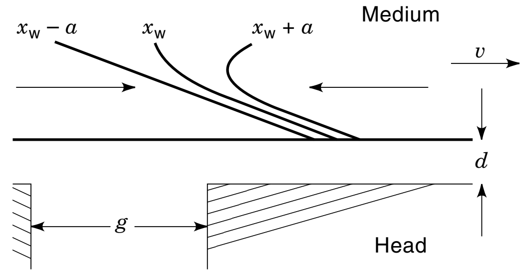

Figure 18. Sketch of transition center and width as function of depth for recording on acicular particulate media. The transition shape is not vertical due to geometrical effects.

prevent the head field from catching all of the switched particles again).

The slope model described so far holds for the thin-film approximation. Since tape, including ME tape, is a 'thick' recording medium, no one-dimensional model can describe tape recording well. Middleton et al. have suggested to decompose a thick medium into laminae, which themselves can be treated using the thin-film approximation (75). Other workers utilized the idea and several models have been developed, which yield results remarkably close the numerical models (70,76,77). Each sublayer is treated conventionally, but has a different magnetization, transition center and transition parameter. The magnetic interaction between the sublayers has to be calculated using Eqs. (35), (36), and (38).

Figure 18 illustrates a typical transition shape as it occurs for longitudinal MP tape. The three lines indicate how the transition shape varies as function of depth. The middle line gives the change of the transition center with depth, $x_w(z')$, and the other two lines show $x_w(z') \pm a(z')$ indicating the transition width. The demagnetization can broaden the transition by either increasing the transition tilt or increasing $a(z')$. Details depend on the angle dependence of the switching field, that is, the recording geometry. Figure 18 also helps to understand the recording behavior of thin-layer MP tapes. In a thin-layer MP tape, the parts of the medium far away from the head do not exist. The existence or nonexistence of the deeper layers does not have a first-order effect on what happens in the upper part of the medium, since geometric effects rather than magnetic effects dominate the recording. Theory and experiment indeed did not show significant changes in recording output for short wavelength for thick- and thin-layer MP tape (7,70). As expected, the thin MP tape shows higher overwrite and lower output at long wavelength. As a consequence of the reduced layer thickness, the saturation curves for thin-layer MP tape show a broader maximum, which is a second-order effect.

Modeling of ME tape is more difficult than modeling of longitudinal tape. Cramer has developed a numerical model for ME tape that is very successful (78). Stupp et al. report a simple multilayer slope model for ME tape, which agrees well with Cramer's numerical model (76). Although similar and successful for longitudinal tape, Richter's model failed for ME tape (70). The two slope models solve the nonlinear equations differently. This seemingly trivial detail directed the solution such that the transition shape follows the column inclination for the successful model. The unsuccessful model ended up with a different transition shape similar to that reported in

Ref. 69. In hindsight, the correct explanation is that there is a magnetic correlation in ME tape that forces the transition to follow the columns. The iteration used in the successful model implicitly assumes this correlation. The existence of such a correlation is consistent with noise investigations (79).

Noise

At playback, the reading head senses a limited volume of the tape. The average magnetization of all magnetic particles in that volume determines the signal. The deviation from the mean magnetization is noise. The more particles are contained in the sensing volume, the smaller the deviations of the mean, and the larger the signal-to-noise ratio, SNR, will be. Simple statistical arguments indicate that the (power) SNR is proportional to the number of particles per unit volume. Since the particles are much smaller than the recording dimensions, *particulate noise,* as described above, is approximately additive.

Particulate noise had been regarded as independent from the magnetization state for a long time. Today it is known that the particulate noise contribution should be largest when the medium is not magnetized, that is, the noise is maximum at the magnetization transitions. Therefore, the noise is not *stationary.* Tape media—including ME tape—have a relatively small volumetric packing fraction, typically smaller than 50%. According to Mallinson, the wide-band signal-to-noise ratio is (80):

$$\mathrm{SNR} \approx \frac{\overline{m}^2 n W \lambda^2}{2\pi(1 - p\overline{m}^2)} \qquad \overline{m} = \overline{M}/M_\mathrm{r} \tag{48}$$

where λ is the minimum wavelength occurring in the recording system, $\overline{M}$ is the mean magnetization sensed by the head, p is the volumetric packing fraction of the tape, and n is the number of particles per unit volume. The tape volume sensed by the head is proportional to $W\lambda^2$, which directly appears in Eq. (48). Due to the relatively small packing fraction, the nonstationarity of the noise is removed, to some extent.

While Eq. (48) predicts the noise to be largest in an ac state, experiment shows that most tapes are noisiest when dc erased. Other noise sources cover the (uncorrelated) particle noise (64). Clusters of particles that have not been separated during the dispersing process and surface roughness effects are reasons for this additional noise.

Especially for particulate tape, *modulation noise* is of great interest. Modulation noise is multiplicative in nature: the noise becomes larger with larger signal. It occurs when the size of the noise sources is no longer small compared with the trackwidth. In practice, it is most difficult to achieve a very smooth surface that successfully eliminates modulation noise. Long wavelength modulation noise is easily recognized in a noise spectrum by the skirts around the signal, or *carrier* (64). In digital recording, modulation noise causes the error rate performance to deteriorate (81). In analog recording, the modulation noise interferes with the modulated signals to be recorded.

Analog Audio Recording (Ac Bias)

Analog audio recording aims directly to reproduce the sound waves of music or speech as a magnetization pattern on a tape. The human ear is sensitive to frequencies between 20 Hz and 20 kHz, and the faithful reproduction of music requires a bandwidth of 50 Hz to 15 kHz. This very large frequency ratio means that the recording conditions are very different from those for digital systems.

In the ubiquitous compact cassette (CC) format, the tape speed is 4.75 cm/s, and the wavelengths corresponding to 50 Hz and 15 kHz are 950 μm and 3.2 μm, respectively. Considering the ‘thickness loss’ term, Eq. (43), the appropriate depths of recording for these two signals would be ~300 μm and ~1 μm. A second distinguishing feature of the analog tape system is that the system needs to have a linear amplitude response. This requirement conflicts with the essentially nonlinear mechanism of magnetic remanence, so a linearizing process is necessary. In early tape recorders, a dc bias was added to the signal. In the magnetization versus field diagram, this serves to move the recording point to the nearly straight part of the isothermal remanence curve close to the coercivity (Fig. 19). The bottom of Fig. 19 illustrates that the zero signal level moves to a finite depth of recording. The great disadvantage of this procedure is that the upper layers of the tape are magnetically saturated, but have no signal contribution and high noise. The addition of a large high-frequency dither signal is therefore the method now universally used. Although the dither signal is symmetrical, it is, perhaps unfortunately, termed *ac bias,* in analogy to the dc bias described above. It will be seen that the application of the dither signal can be understood as an anhysteretic magnetization process. Figure 19 shows that the anhysteretic remanence curve (labeled M_ar) is more sensitive to signal than the dc biased IRM curve. Most importantly, the anhysteretic remanence is symmetrical about the origin, which assigns zero signal to a demagnetized tape, that is, zero signal is associated with low noise.

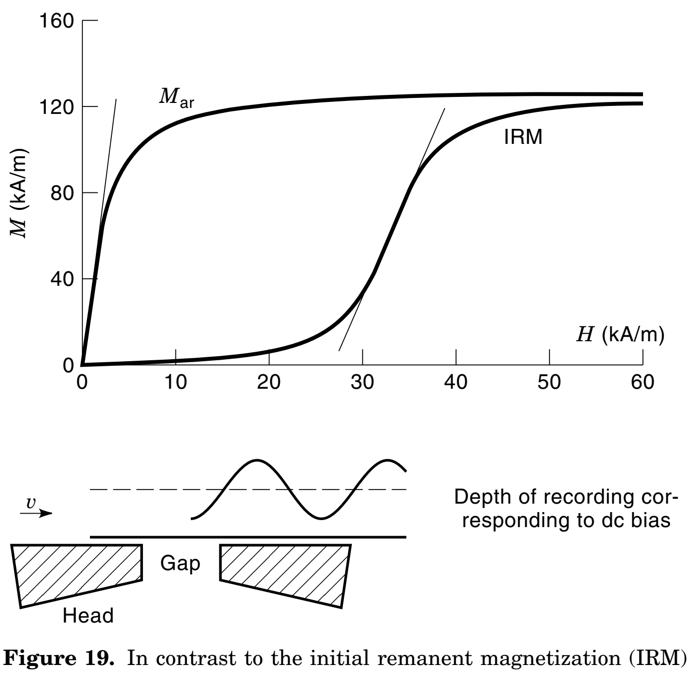

Figure 19. In contrast to the initial remanent magnetization (IRM) curve, the more linear anhysteretic remanence curve assigns zero magnetization to zero signal (or field). The bottom figure shows that dc bias, which would be required to linearize the IRM curve, results in a writing depth modulation.

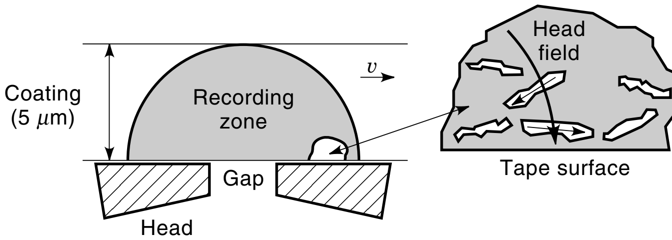

Figure 20. Recording zone for ac-bias recording. Due to the overbiasing of the short wavelengths, the head field relevant for the recording is almost vertical, which tends to demagnetize the tape.

Figure 20 shows the essential recording geometry of a standard cassette recorder. The recording gap is typically 2 μm and the coating thickness 5 μm. In order to use the full tape thickness for maximum long wavelength response, the bias is set to write through the entire magnetic coating. This means that the head current and depth of recording are set far too high for optimum recording of the highest frequencies. The enlargement of Fig. 20 illustrates one negative consequence of this overbiasing: near the surface, the head field relevant for the switching is almost vertical. Thus, there is a tendency to demagnetization, because differently inclined particles are magnetized in different directions. This mechanism is identical to that leading to the double transitions in ME tape, as previously described. Improved orientation of the particles diminishes this effect.

Two important performance parameters are the maximum output level (MOL) and the saturation output level (SOL). In the CC system, MOL is the 333 Hz output at which the third harmonic distortion reaches 3%, and the SOL is the maximum output attainable at 10 kHz. MOL and SOL are shown as function of the ac bias current in Fig. 21, confirming that at the specified bias, MOL is not far from its maximum and that the 10 kHz signal is grossly overbiased. Variations in tape coercivity mirror the dependence on bias current, so, because the bias current is set for the recorder, the coercivity must be tightly controlled. Presumably, this high sensitivity to coercivity has led to a general overestimation of the importance of coercivity in magnetic recording.

Applying the ac bias signal of 80 kHz to 100 kHz corresponds to an attempt to write a wavelength of about 0.5 μm onto the tape. An audio recorder is not designed to record such a short wavelength and the bias signal is heavily

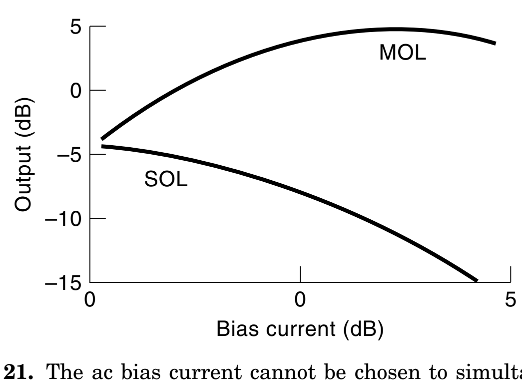

Figure 21. The ac bias current cannot be chosen to simultaneously optimize both the Maximum Output Level (MOL) and the Saturation Output Level (SOL).

damped. Instead of modeling a long sequence of blurred bias frequency transitions, it is usual to subsume the ac signal into the magnetic properties of the tape and treat the recording process as one of anhysteretic magnetization at the signal wavelengths. Anhysteretic magnetization is the process by which to a small offset field is added a large ac. The ac (bias) field is slowly reduced to zero from a large value sufficient to switch all the particles. The sample traverses many hysteresis cycles, destroying the memory of any previous magnetization and converging on a single-valued function of the offset field. [Anhysteretic magnetization does not quite correspond to ac bias recording: while the offset field remains constant for anhysteretic magnetization, it decays together with the ac field in a recording. This *modified anhysteretic process* is similar to the anhysteretic process (82).] Anhysteretic magnetization, M_a, with the offset field applied is always higher than anhysteretic remanence, M_{ar}, with the offset field removed. The difference between the two is small along the recording direction of well-oriented tapes, and M_{ar} will stand for both in the following discussion. The initial slope of the curve is called the *anhysteretic remanent susceptibility,* χ_{ar}, and the main task is to explain its finite value. If the ac field is reduced sufficiently slowly, that is, the decrement ΔH_{ac} between subsequent half cycles is smaller than the magnitude of the signal field, all particles must be magnetized in the direction of the signal field. Therefore, one expects χ_{ar} to be infinite, which is in contradiction with experiment (see Fig. 19). One reason for χ_{ar} to be finite is that thermal activation introduces statistical uncertainty in particle switching, but the effect is rather small. For magnetic tapes, which are rather densely packed, the effects of interparticle magnetic interactions dominate. A graphical way to explain the effect of these interactions is the Preisach diagram (83), a version of which is shown in Fig. 22. The Preisach diagram is a particle density plot. In the representation used here, the strength of the Preisach function is indicated by the contours shown in

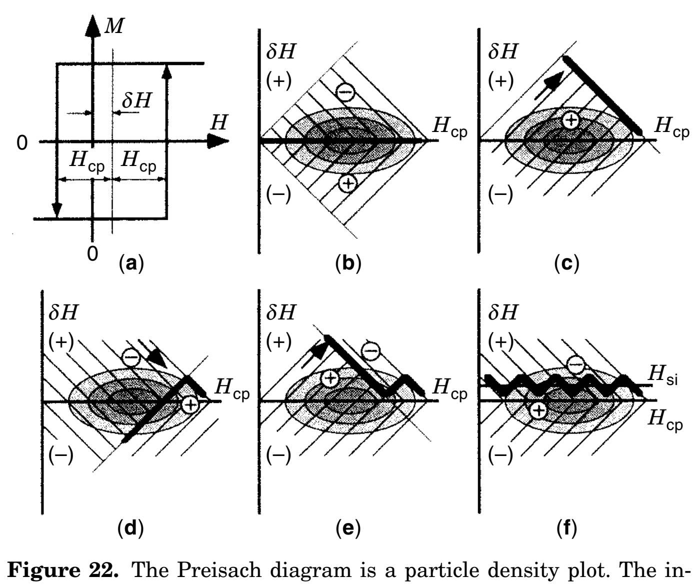

Figure 22. The Preisach diagram is a particle density plot. The intrinsic coercivity, H_{cp}, is on the abscissa and the interaction field, δH, is on the ordinate. The interaction field δH shifts the hysteresis loop (a). Depending on whether the applied field is increasing or decreasing, the boundary between the particles, which can and cannot be switched, is oriented at 45° or 135°.

Figs. 22(b)–22(f). The abscissa of the Preisach diagram gives the intrinsic particle coercivity, H_{cp}, without any interaction, while the ordinate represents the (magnetostatic) interaction field, δH, which the particle experiences. δH is created by all the other particles. As Fig. 22(a) illustrates, a positive interaction field δH shifts the hysteresis loop to the right. A decaying ac bias field will thus always negatively magnetize particles with positive interaction field, and vice versa. Figure 22(b) shows a representation of an ideally erased state ($M = 0$), with equal populations magnetized in either direction.

Consider now an increasing field applied to the (demagnetized) particle assembly. The negatively magnetized particles can switch to positive magnetization, if the applied field, H_a, is bigger than the coercivity augmented by the interaction field: $H_a > H_{cp} + \delta H$. Since $\delta H > 0$ for the negatively magnetized particles, the applied field can remagnetize all particles below $H_a = H_{cp} + \delta H$, which is the heavy line shown in Fig. 22(c). If the applied field is decreased again, those particles can switch back to negative magnetization, for which holds: $H_a > H_{cp} - \delta H$. In this case the terminating line rotates by 90°, as indicated in Fig. 22(d). Continuing the field sequence leaves a net magnetization without saturating the sample as in the interaction free discussion above [(Figs. 22(e) and (f)]. In small offset fields, H_{Si}, the magnetization is proportional to the density of particles near the H_{cp} axis. Thus, the Preisach representation qualitatively accounts for the finite χ_{ar}. The reader can find more detail in Refs. 58, 65, 84, 85.

While the Preisach model qualitatively describes magnetic interaction effects, it remains unsatisfactory, because the nature of the interaction is an assumption rather than a natural consequence of the model. In contrast to the Preisach model that merely assumes "positive" or "negative" interactions, Kneller (86) calculated the mean interaction field including structural information. He treated magnetic interaction as a *dynamic* interaction field, which is controlled by the magnetization. Using this concept, Kneller et al. calculated the anhysteretic susceptibility for an ensemble of infinite cylindrical particles (87):

$$\chi_{ar} = \frac{0.5p(1-p)M_s^2}{H_r^2(1-S_q^2)} \tag{49}$$

After empirically replacing the factor 0.5 with 0.27 to account for SFD > 0, Eq. (49) is in good agreement with experiment. Köster (88) also found that to a good approximation, the M_{ar} curves of all oriented tape samples followed the universal relationship

$$\frac{M_{ar}}{M_r} = 0.569\frac{H}{H_{ar}} - 0.0756\left(\frac{H}{H_{ar}}\right)^3 + 0.0065\left(\frac{H}{H_{ar}}\right)^5 \tag{50}$$

where H_{ar} is the offset field for which M_{ar} becomes 50% of the saturation remanence M_r. Using this expression, 3% MOL corresponds to a magnetization $M_r/2$; linearity has been bought at the expense of using only half of the potential magnetization and dynamic. The orientation and SFD have a subordinated but still important beneficial influence on the linearity and, of course, better orientation increases M_r.

Bertram (89) using the anhysteretic model calculated the magnetization profile in the tape coating and found, because at the tape surface the head field is almost perpendicular, the magnetization increased with depth into the tape. Details depend on the angular switching behavior of the particles and the degree of orientation. Generally, higher orientation and M_r, together with narrower SFD, improve the output, while the correct balance between MOL and SOL is set by the coercivity.

Further Aspects of Recording

- *Erasure and Overwrite.* The hysteresis energy dissipated in recording a magnetic transition is sufficient to cause local heating of 0.1 K. Consequently, there is no physical or chemical damage to the tape and, from the magnetic standpoint, the tape may be rerecorded infinitely often. In order to reuse the tape, however, the old information must be erased. When the recording head itself is used for this purpose, several difficulties arise, owing to the small spatial extent of the head field. Clearly, if the head is incorrectly positioned or lifted from the tape surface by a speck of dirt, then the field will not reach all parts of the written track. A more subtle effect arises because the head field zone is so narrow that it is bridged by the field emanating from the unerased portion of the tape. In ac-bias recording, it has been shown (90) that even the tape noise can in this way be rerecorded and amplified leaving the so-called bias noise 3 dB above the true statistical particle noise. Analog recorders therefore always carry additional erase heads with gaps 5 to 10 times that of the recording head. Bulk erasure gives good results and is one of the last steps in tape manufacturing, where it is necessary to remove the magnetization induced by the orienting magnet as well as any control signal used by the processing equipment. The magnetic annealing effect in some cobalt-modified iron oxide tapes can hinder erasure [a 20 dB increase in residual signal was reported in (91)]. In digital recording, the old information is often overwritten directly. Overwriting is a very complex process: apart from incomplete erasure, the old information modulates the new information being written and complicated interference phenomena can occur. For improving overwrite behavior, a narrow SFD is beneficial. The different materials differ in overwrite behavior. In case of particulate media, Co-doped γ-Fe_2O_3 and BaFe are most difficult to overwrite, γ-Fe_2O_3 and MP are better to overwrite, and CrO_2 is best. ME tape outperforms all particulate media, which is due to the narrow SFD and the perpendicular magnetization component.
- *Writing Spacing Loss.* This adds to the reading spacing loss. The total spacing loss for acicular tape media is about 100 dB d/λ which agrees well with theory (69,70). The writing spacing loss is smaller in thin magnetic layers.
- *Length Loss.* If the length of the particles approaches the wavelength of interest, the output decreases:

$$\mathrm{LL} = \frac{\sin(\pi L/\lambda)}{\pi L/\lambda} \tag{51}$$

This analysis assumes the length loss to be independent of the recording process. Obviously, the transition parameter cannot become smaller than L/π, which has to be considered at the writing process. For investigations on Length Loss, see Refs. 92–94.

- At writing, transitions in longitudinal recording are shifted away from the gap due to the effect of the demagnetizing field of the previous transition. Similarly, transitions in vertical recording are drawn closer to the gap. Therefore Mallinson suggested that media with an oblique easy axis—ME tape—could eliminate the *nonlinear transition shift,* that is, the shift due to demagnetization (95). Later it was proven experimentally, that there is indeed an inclination angle of the easy axis that eliminates nonlinear transition shift (96).

RECORDING SYSTEMS

Linear Recorders

The number and variety of recording systems is huge. One can classify the recording systems into analog and digital or into linear and helical-scan systems. An example for an analog *linear recorder* is a tape deck. Figure 23 shows the basic mechanism of a linear tape recorder. After unwinding, the tape passes by an erase head, a recording head, and a replay head. Alternatively, one head can operate as both the recording and the replay head. All heads are stationary. The erase head has a large gap length that ensures full erasure of the tape. The tracks in such a recorder are parallel to the tape running direction, which gives the linear recorder its name. In audio recorders, the tracks 1 and 3 are used to run in one direction, and tracks 2 and 4 are used in the other. This minimizes crosstalk. Open-reel tape systems for audio recording operate in a linear mode. In 1963, Philips invented the compact cassette as an alternative for the bulky and difficult-to-handle open-reel tape recorders. The compact cassette systems have smaller dimensions and a lower head-to-medium speed, which sacrifices performance. Later, better tapes, heads, and electronics made up for the performance loss. Table 2 lists some magnetic properties of IEC I (standard compact cassette tape), and IEC II (improved compact cassette tape). The magnetic material in IEC II is CrO_2 or Co-doped γ-Fe_2O_3, while IEC I tape utilizes γ-Fe_2O_3 particles.

The tape speed and the minimum achievable wavelength determine the data rate or the maximum frequency of a linear recorder. Since high tape speed is undesirable because of high tape consumption, the frequency response of a linear recorder suffers. In order to increase the data rate, several heads can be operated in parallel. The operation of parallel channels requires a good head-to-tape contact over a large region, which is difficult to achieve. An example for a system that operates successfully nine parallel tracks is the digital compact cassette (DCC) system.

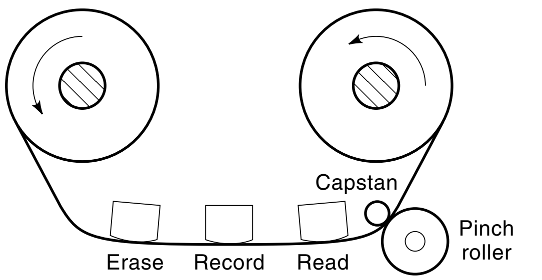

Figure 23. Sketch of a linear recorder with three heads.

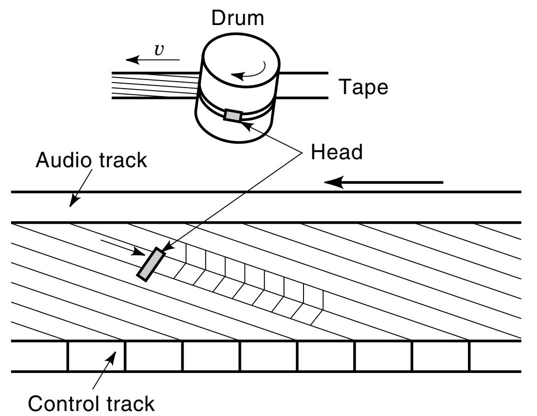

Figure 24. Helical scan principle: The tilted head drum records slanted tracks on the medium. The tape movement and the drum rotation are two independent, but simultaneous motions. The magnetization directions of adjacent tracks show an additional tilt (azimuth recording) to prevent side reading.

Helical-Scan Recorders

High-frequency applications such as video recorders use the helical-scan principle. In contrast to the linear recorders, the heads in helical-scan recorders are not stationary but mounted on a drum. There are two simultaneous motions in a helical-scan recorder: (1) the tape moves with a constant, relatively slow speed (few centimeters per second), and (2) the head drum rotates with a high speed (several meters per second). The axis of the head drum is not oriented parallel to the transverse direction, but it is tilted by a small angle. This results in slanted written tracks. Figure 24 shows a sketch of the recording configuration as well as a typical track format on the tape for a VHS recorder.

Analog video is always recorded using frequency modulation. Frequency modulation is chosen because it is insensitive to the amplitude changes caused by small surface variations at such short wavelengths. The modulated signal is amplitude limited and looks just like a digital signal. Demodulating the signal involves detecting the zero-crossings of the output signal, so again there is great similarity to digital techniques. Helical-scan became universal after several failed attempts to build mechanically sound high-velocity linear drives.

As Fig. 24 indicates, the head is wider than the spacing between the tracks (*track pitch*). Consequently, the head will always read a portion of the adjacent track(s). To prevent crosstalk, the gap orientations of the recordings of adjacent tracks are tilted against one another. This is called *azimuth recording.* Tilting the writing direction against the reading direction by an angle β reduces the output:

$$L = \frac{\sin\left(\frac{\pi W}{\lambda}\tan\beta\right)}{\frac{\pi W}{\lambda}\tan\beta} \tag{52}$$

Azimuth recording thus requires at least two heads on the head drum. The two heads with different azimuth angle record and read alternately. In analog video systems, the length of the track corresponds to one field or half picture. Therefore, the recorder can produce a picture (*still-frame*) without any tape motion. Achieving a reliable still-frame operation is one of the most challenging tasks for a tape manufacturer. For tracking, there is often (a) control track(s), as indicated in Fig. 24.

The audio track shown in Fig. 24 is recorded using standard ac bias with a stationary head (see the section titled Analog Audio Recording). Due to the very low tape speed, the quality of the audio recording is poor. Recording the frequency modulated (FM) audio information with the rotating head improves the audio quality significantly. The audio information is recorded in a separate frequency band. In case of VHS, the audio information is first recorded using a large gap head and subsequently overwritten with the video information. The video information is recorded with a head with small gap length and occupies only a very shallow layer. This suffices for the short wavelength region relevant for the video signal. On the other hand, the audio signal remains essentially untouched.

The most important analog consumer video systems are VHS, S-VHS (Super-Video Home System), 8 mm and Hi 8. Other systems (e.g., Video 2000, Betamax) did not penetrate the market. The next consumer video system is DVC (digital video cassette), which is the counterpart to DVD (digital video disk). Professional recorders for broadcasting (such as D1 to D5, DVC-Pro, Betacam SP and digital Betacam) are similar in principle, but considerably more complex than the consumer devices with up to 32 different heads on one single drum. Most of these systems have NTSC (National Television System Committee) and PAL (phase alternating line) versions. The PAL and NTSC versions differ not only in the technology directly related to the broadcasting schemes, but also slightly in recording density and sometimes even in tape grade. Table 3 summarizes some data for the most important recording systems. Although several tape materials can be used for one system, switching between different types may not be advisable. The video heads stick out of the drum somewhat. Therefore, the head is pressed into the tape, which then forms a "tent." Mechanically, each head contours itself with time such that the head-to-medium contact is optimal. Changing the tape material may have the effect that the contouring process starts again from the beginning.

The new digital video systems show a new trend in storage philosophy. Not too long ago, it seemed mandatory that digital tape systems should store the full information. Digital Betacam and the DVC system utilize data-compression schemes. In contrast to audio or even data information, video information is highly redundant. Today much effort is directed toward identifying redundant information and to process the relevant data as economically as possible. Data compressions can reduce the amount of data by a factor of up to 50, without noticeable quality loss. This does not eliminate the need for higher recording density, since the playing times are still limited, even with data compression. It should be mentioned that helical scan recorders, derived from digital audio and video systems, are also used in digital data storage (DDS) systems.

Videotape Duplication. Most of the videotape produced enters the market as prerecorded tape. It is not attractive to record these tapes at the normal speed of a video recorder. There are two principles that allow to record videotape at much higher speed. In case of *thermal duplication,* the video information is recorded onto a CrO_2 tape. CrO_2 has a very low Curie temperature (120°C). At duplication, the CrO_2 tape is heated up to the Curie temperature and subsequently cooled down with a master tape in direct contact to it. At the cooling process, the magnetic pattern of the master—MP or Co-doped γ-Fe_2O_3 tape—is imprinted onto the slave. The duplication process can be very fast, if the tape is heated with a laser. CrO_2 is the only material suitable for thermal duplication. Another method for duplication is *anhysteretic duplication.* In this case, the master and the slave tape are subjected to an alternating transfer field while they are in contact. The master tape has about three times the coercivity as the slave and is recorded in a mirror image. The recording process is very similar to ac bias recording. The decaying alternating field takes the role of the ac bias and the stray field—which is added, as in ac bias recording—contains the information to be recorded. For further reading, see Refs. 85, 97–99.

MAGNETIC TAPE RECORDING: OUTLOOK

Magnetic recording and, in particular, magnetic tape recording, is a very old technology. The principles of magnetic

Table 3. Characteristic Data of Some Recording Systems

System		TW (mm)	TP (μm)	BL (μm)	AD (bit/μm^2)	Thickness (μm)
VHS	Analog video (PAL)	12.7	49	0.51	0.04	20
	Analog video (NTSC)	12.7	58	0.66	0.03	20
S-VHS	Analog video (PAL)	12.7	49	0.35	0.06	20
	Analog video (NTSC)	12.7	58	0.42	0.04	20
8 mm	Analog video (PAL)	8	34	0.29	0.10	10
	Analog video (NTSC)	8	20	0.35	0.14	10
Hi 8	Analog video (PAL)	8	34	0.21	0.14	10
	Analog video (NTSC)	8	20	0.25	0.20	10
R-DAT	Digital Audio	3.81	13.5	0.41	0.18	10
DVC	Digital video	6.35	10	0.24	0.42	7
HD, 1.4 MB	Floppy disk	—	188	1.46	0.0036	67
100–120 MB	Floppy disk	—	10	0.75	0.13	67
Data tape	Cartridge, 1998	8	69	0.32	0.046	~7
		6.35	34	0.5	0.06	~7

TW: tape width, TP: track pitch, BL: transition spacing, AD: areal density, and thickness of the tape/disk. Analog systems are converted for comparison, track pitch is given for short-play mode.

recording on particulate recording tape are well established, since the middle of 1940s. Since then, the technology has followed an evolutionary rather than a revolutionary path. Decreasing the particle size, narrowing the particle size distribution, and improving the manufacturing technology has resulted in considerably improved tape performance. The main path for future *particulate tape* is MP. To date, *thin-film* tape (ME tape) has shown the best recording performance. ME tape has been commercially available since the beginning of the 1990s. Present estimates indicate that both types of media, particulate and thin film, can support significantly higher areal storage density than those already demonstrated (7).

While the recording performance data indicate that the difference between thin-film media and particulate media is moderate, thin-film media may take advantage of their physical 'thinness'. The coating thickness of particulate tapes cannot be made smaller than 1 μm or 2 μm. This also holds for the double-layer tapes, which have a thin magnetic layer, but require a fairly thick (1 μm to 2 μm) underlayer. Base films can be as thin is 5 μm or even less. The thickness of the two layers adds much more to the total thickness of a tape than the thin metal film does. In the end, more tape fits into a cassette, which favors thin-film tape.

Magnetic tape recording offers very large storage capacity per volume at low cost. While the data rates are high, the access times are longer when compared with recording technologies that use disk-shaped media. These features make tape ideally suited for applications in which access time can be traded off against storage capacity.

BIBLIOGRAPHY

1. E. Köster, Particulate Media, in C. D. Mee and E. D. Daniel (eds.), *Magnetic Recording Handbook,* 2nd ed., New York: McGraw-Hill, 1996.
2. H. Jakusch and R. J. Veitch, Paticles for magnetic recording, *J. Inf. Rec. Mats,* **20**: 325–344, 1993.
3. M. P. Sharrock, Particulate magnetic recording media: A review, *IEEE Trans. Magn.,* **25**: 4374–4389, 1989.
4. G. Bate, Magnetic recording materials since 1975, *J. Magn. Magn. Mat.,* **100**: 413–424, 1991.
5. E. Schwab and H. Hibst, Magnetic recording materials, in R. Cahn, P. Haasen and E. Kramer (eds.), *Materials Science and Technology,* Vol. 3B, Weinheim: VCH, Verlagsgesellschaft, 1993.
6. H. Inaba et al., The advantages of the thin magnetic layer on a metal particulate tape, *IEEE Trans. Magn.,* **29**: 3607–3612, 1993.
7. H. J. Richter and R. J. Veitch, Advances in magnetic tapes for high density information storage, *IEEE Trans. Magn.,* **31**: 2883–2888, 1995.
8. S. Saitoh, H. Inaba, and A. Kashiwagi, Developments and advances in thin layer particulate recording media, *IEEE Trans. Magn.,* **31**: 2859–2864, 1995.
9. K. Shinohara et al., Columnar structure and some properties of metal evaporated tape, *IEEE Trans. Magn.,* **20**: 824–826, 1984.
10. T. Kawana, S. Onodera, and T. Samoto, Advanced metal evaporated tape, *IEEE Trans. Magn.,* **31**: 2865–2870, 1995.
11. M. S. Cohen, Anisotroy in Permalloy films evaporated at grazing incidence, *J. Appl. Phys.* Suppl., **32**: 87S–88S, 1961.
12. J. M. Alameda, M. Torres, and F. López, On the physical origin of in-plane anisotropy axis switch in oblique-deposited thin films, *J. Magn. Magn. Mat.,* **62**: 209–214, 1986.
13. H. J. Richter, An analysis of magnetization processes in metal evaporated tape, *IEEE Trans. Magn.,* **29**: 21–33, 1993.
14. A. G. Dirks and H. J. Leamy, Columnar microstructure in vapor-deposited thin films, *Thin Solid Films,* **47**: 219–233, 1977.
15. G. Bottoni, D. Gandolfo, and A. Ceccetti, Exchange anisotropy in metal evaporated tape, *IEEE Trans. Magn.,* **30**: 3945–3947, 1994.
16. Y. Kaneda, Tribology of metal evaporated tape for high density magnetic recording, *IEEE Trans. Magn.,* **33**: 1058–1068, 1997.
17. R. Sugita et al., Incident angle dependence of recording characteristics of vacuum deposited Co-Cr films, *IEEE Trans. Magn.,* **26**: 2286–2288, 1990.
18. Y. Maeda, S. Hirono, and M. Asahi, TEM observation of micro-structure in sputtered Co-Cr film, *Jpn. J. Appl. Phys.,* **24**: L951–L953, 1985.
19. Y. Maeda and M. Asahi, Segregation in sputtered Co-Cr films, *IEEE Trans. Magn.,* **23**: 2061–2063, 1987.
20. K. Ishida and T. Nishizawa, The Co-Cr (cobalt-chromium) system, *Bull. Alloy Phase Diag.,* **11**: 357–369, 1990.
21. J. E. Snyder and M. H. Kryder, Quantitative thermomagnetic analysis of CoCr films and experimental determination of the CoCr phase diagram, *J. Appl. Phys.,* **73**: 5551–5553, 1993.
22. Y. Nakamura and S. Iwasaki, *Perpendicular magnetic recording method and materials,* Magnetic Materials in Japan: Research, Applications and Potential, Japan Technical Information Service, Elsevier, pp. 4–106, 1991.
23. E. Köster, Recommendation of a simple and universally applicable method for measuring the switching field distribution of magnetic recording media, *IEEE Trans. Magn.,* **20**: 81–83, 1984.
24. J. P. C. Bernards and H. A. J. Cramer, Vector magnetization of recording media: A new method to compensate for demagnetizing fields, *IEEE Trans. Magn.,* **27**: 4873–4875, 1991.
25. J. U. Lemke, An isotropic particulate medium with additive Hilbert and Fourier field components, *J. Appl. Phys.,* **53**: 2561–2566, 1982.
26. E. C. Stoner and E. P. Wohlfarth, A mechanism of magnetic hysteresis in heterogeneous alloys, *Trans. R. Soc.,* **A240**: 599–642, 1948.
27. I. S. Jacobs and C. P. Bean, An approach to elongated fine-particle magnets, *Phys. Rev.,* **100**: 1060–1067, 1955.
28. Y. Ishii and M. Sato, Magnetic behaviors of elongated single-domain particles by chain-of-spheres model, *J. Appl. Phys.,* **59**: 880–887, 1986.
29. A. Aharoni, Nucleation of magnetization reversal in ESD magnets, *IEEE Trans. Magn.,* **5**: 207–210, 1969.
30. W. F. Brown, Jr., Criterion for uniform micromagnetization, *Phys. Rev.,* **105**: 1479–1482, 1957.
31. E. H. Frei, S. Shtrikman, and D. Treves, Critical size and nucleation field of ideal ferromagnetic particles, *Phys. Rev.,* **106**: 446–455, 1957.
32. W. F. Brown, Jr.,, *Magnetostatic Principles in Ferromagnetism,* Amsterdam: North-Holland, 1962.
33. W. F. Brown, Jr., Micromagnetism, Recent Advances in Engineering Sciences, 5, of *Proc. 6th Tech. Meeting Soc. Eng. Sci.,* London: Gordon and Breach, 1970, pp. 217–228.
34. W. F. Brown, Jr., *Micromagnetics,* Huntington, NY: Krieger, 1978.
35. A. Aharoni, Some recent developments in micromagnetics at the Weizmann Institute of Science, *J. Appl. Phys. Suppl.,* **30**: 70S–78S, 1959.
36. A. Aharoni, Perfect and imperfect particles, *IEEE Trans. Magn.,* **22**: 478–483, 1986.
37. H. J. Richter, Media requirements and recording physics for high density magnetic recording, *IEEE Trans. Magn.,* **29**: 2185–2201, 1993.

38. A. Aharoni, Nucleation modes in ferromagnetic prolate spheroids, *J. Physics: Condensed Matter,* **9**: 10009–10021, 1997.
39. M. E. Schabes, Micromagnetic theory of non-uniform magnetization processes in magnetic recording particles, *J. Magn. Magn. Mat.,* **95**: 249–288, 1991.
40. S. Shtrikman and D. Treves, The coercive force and rotational hysteresis of elongated ferromagnetic particles, *J. Phys. Rad.,* **20**: 286–289, 1959.
41. A. Aharoni, Magnetization curling, *Phys. Stat. Sol.,* **16**: 3–42, 1966.
42. W. F. Brown, Jr., The Theory of Thermal and Imperfection Fluctuations in Ferromagnetic Solids, in R. E. Burgess (ed.), *Fluctuation Phenomena in Solids,* New York: Academic Press, 1965.
43. E. F. Kneller and F. E. Luborsky, Particle size dependence of coercivity and remanence of single-domain particles, *J. Appl. Phys.,* **34**: 656–658, 1963.
44. M. P. Sharrock and J T. McKinney, Kinetic effects in coercivity measurements, *IEEE Trans. Magn.,* **17**: 3020–3022, 1981.
45. L. He, D. Wang, and W. D. Doyle, Remanence coercivity of recording media in the high speed regime, *IEEE Trans. Magn.,* **31**: 2892–2894, 1995.
46. L. He et al., High-speed switching in magnetic recording media, *J. Magn. Magn. Mat.,* **155**: 6–12, 1996.
47. W. F. Brown, Thermal fluctuations of a single-domain particle, *Phys. Rev.,* **130**: 1677–1686, 1963.
48. D. P. E. Dickson et al., Determination of f_0 for fine magnetic particles, *J. Magn. Magn. Mat.,* **125**: 345–350, 1993.
49. R. H. Victorla, Predicted time dependence of the switching field for magnetic materials, *Phys. Rev. Lett.,* **63**: 457–460, 1989.
50. E. P. Wohlfarth, The coefficient of magnetic viscosity, *J. Phys. F,* **14**: L155–L159, 1984.
51. R. Street and J. C. Woolley, A study of magnetic viscosity, *Proc. Phys. Soc.,* **A62**: 562–572, 1949.
52. H. Jachow, E. Schwab, and R. J. Veitch, Viscous magnetization of chromium-dioxide particles: Effect of increased magnetocrystalline anisotrophy, *IEEE Trans. Magn.,* **27**: 4672–4674, 1991.
53. R. J. Veitch et al., Thermal effects in small metallic particles, *IEEE Trans. Magn.,* **30**: 4074–4076, 1994.
54. E. D. Daniel and P. E. Axon, Accidental printing in magnetic recording, *BBC Q.,* **5**: 214–256, 1951.
55. J. C. Mallinson and H. N. Bertram, A theoretical and experimental comparison of the longitudinal and vertical modes of magnetic recording, *IEEE Trans. Magn.,* **20**: 461–467, 1984.
56. J. R. Desserre, Crucial points in perpendicular recording, *IEEE Trans. Magn.,* **20**: 663–668, 1984.
57. R. L. Wallace, Jr., The reproduction of magnetically recorded signals, *Bell Syst. Tech. J.,* **30**: 1145–1173, 1951.
58. W. K. Westmijze, Studies on magnetic recording, parts 1–5, *Philips Res. Rep.,* **8**: 148–157; 161–183; 245–255; 255–269; 343–354; 1953.
59. J. C. Mallinson, On the properties of two-dimensional dipoles and magnetized bodies, *IEEE Trans. Magn.,* **17**: 2453–2460, 1981.
60. H. N. Bertram, Fundamentals of the magnetic recording process, *Proc. IEEE,* **74**: 1494–1512, 1986.
61. J. J. M. Ruigrok, *Short-wavelength magnetic recording,* Eindhoven: Elsevier, 1990.
62. O. Karlqvist, Calculations of the magnetic field in the ferromagnetic layer of a magnetic drum, *Trans. Roy. Soc. Techn. (Stockholm),* **86**: 1–27, 1954.
63. T. J. Szczech, D. M. Perry, and K. E. Palmquist, Improved field equations for ring heads, *IEEE Trans. Magn.,* **19**: 1740–1744, 1983.
64. H. N. Bertram, *Theory of Magnetic Recording,* Cambridge: Cambridge Univ. Press, 1994.
65. B. K. Middleton, Recording and reproducing processes, in C. D. Mee and E. D. Daniel, (eds.), *Magnetic Recording Handbook,* 2nd ed., New York: McGraw-Hill, 1996, Chap. II.
66. J. C. Mallinson, *The foundations of magnetic recording,* 2nd ed., San Diego: Academic Press, 1993.
67. M. L. Williams and R. L. Comstock, An analytic model of the write process in digital magnetic recording, *AIP Conf. Proc.,* **5**: 738–742, 1971.
68. H. N. Bertram and R. Niedermeyer, The effect of spacing on demagnetization in magnetic recording, *IEEE Trans. Magn.,* **18**: 1206–1208, 1982.
69. H. N. Bertram and I. A. Beardsley, The recording process in longitudinal particulate media, *IEEE Trans. Magn.,* **24**: 3234–3248, 1988.
70. H. J. Richter, A generalized slope model for magnetization transitions, *IEEE Trans. Magn.,* **33**: 1073–1084, 1997.
71. D. L. A. Tjaden and J. Leyten, A 5000:1 scale model of the magnetic recoding process, *Philips Tech. Rev.,* **25**: 319–329, 1964.
72. J. C. Mallinson, One-sided fluxes—a magnetic curiosity?, *IEEE Trans. Magn.,* **9**: 678–682, 1973.
73. H. J. Richter, An approach to recording on tilted media, *IEEE Trans. Magn.,* **29**: 2258–2265, 1993.
74. H. A. J. Cramer et al., Write-field interference in the recording process on Co–Cr media: An experimental study, *IEEE Trans. Magn.,* **26**: 100—102, 1990.
75. B. K. Middleton, A. K. Dinnis, and J. J. Miles, Digital recording theory for thick media, *IEEE Trans. Magn.,* **29**: 2286–2288, 1993.
76. S. E. Stupp, S. R. Cumpson, and B. K. Middleton, A quantitative multi-layer recording model for media with arbitrary easy axis orientation, *J. Magn. Soc. Jpn.,* **18** (Suppl. S1): 145—148, 1994.
77. D. Wei, H. N. Bertram, and F. Jeffers, A simplified model for high density tape recording, *IEEE Trans. Magn.,* **30**: 2739–2749, 1994.
78. H. A. J. Cramer, *On the Hysteresis and the Recording Properties in Magnetic Media,* Ph.D. Thesis, Den Haag: Twente University, 1993.
79. S. E. Stupp and A. B. Schrader, Ac-erased and modulation noise in metal evaporated tape, *IEEE Trans. Magn.,* **31**: 2848–2850, 1995.
80. J. C. Mallinson, A new theory of recording media noise, *IEEE Trans. Magn.,* **27**: 3519–3531, 1991.
81. E. Y. Wu, J. V. Peske, and D. C. Palmer, Texture-induced modulation noise and its impact on magnetic recording performance, *IEEE Trans. Magn.,* **30**: 3996–3998, 1994.
82. E. D. Daniel and I. Levine, Experimental and theoretical investigation of the magnetic properties of iron oxide recording tape, *J. Acoust. Soc. Amer.,* **32**: 1–15, 1960.
83. F. Preisach, Über die magnetische Nachwirkung, *Zeitschrift für Physik,* **94**: 277–302, 1935.
84. C. D. Mee, The physics of magnetic recording, in E. P. Wohlfarth (ed.), *Selected Topics in Solid State Physics,* vol. II, Amsterdam: North Holland, 1964.
85. F. Jørgensen, *The Complete Handbook of Magnetic Recording,* 4th ed., New York: McGraw-Hill, 1996.
86. E. F. Kneller, Magnetic-interaction effects in fine particle assemblies and thin films, *J. Appl. Phys.,* **39**: 945–955, 1968.
87. E. F. Kneller and E. Köster, Relation between anhysteretic and static magnetic tape parameters, *IEEE Trans. Magn.,* **13**: 1388–1390, 1977.
88. E. Köster, A contribution to anhysteretic remanence and AC bias recording, *IEEE Trans. Magn.,* **11**: 1185–1187, 1975.

89. H. N. Bertram, Long wavelength ac bias recording theory, *IEEE Trans. Magn.,* **10**: 1039–1048, 1974.

90. E. D. Daniel, Tape noise in audio recording, *J. Audio Eng. Soc.,* **20**: 92–99, 1972.

91. L. Lekawat, G. W. D. Spratt, and M. H. Kryder, Annealing study of the erasability of high energy tapes, *IEEE Trans. Magn.,* **29**: 3628–3630, 1993.

92. J. C. Mallinson, Maximum signal-to-noise ratio of a tape recorder, *IEEE Trans. Magn.,* **5**: 182–186, 1969.

93. T. Fujiwara, Magnetic properties and recording characteristics of barium ferrite media, *IEEE Trans. Magn.,* **23**: 3125–3130, 1987.

94. H. Auweter, et al., Experimental study of the influence of particle size and switching field distribution on video tape output, *IEEE Trans. Magn.,* **27**: 4669–4671, 1991.

95. J. C. Mallinson, Proposal concerning high-density digital recording, *IEEE Trans. Magn.,* **25**: 3168–3169, 1989.

96. S. E. Stupp and C. R. Cumpson, Experimental and theoretical studies of nonlinear transition shift in metal evaporated tape, *IEEE Trans. Magn.,* **33**: 2968–2970, 1997.

97. C. D. Mee and E. D. Daniel, *Magnetic Storage Handbook,* 2nd ed., New York: McGraw-Hill, Chapters 5–8, 1996.

98. J. R. Watkinson, *The Art of Digital Audio,* Boston/Oxford: Focal Press, 1989.

99. S. B. Luitjens, Magnetic recording trends: Media developments and future (video) recording systems, *IEEE Trans. Magn.,* **26**: 6–11, 1990.

HANS JÜRGEN RICHTER
Seagate Technology

RONALD J. VEITCH
BASF Aktiengesellschaft